



# Facile synthesis of carbon-coated layered double hydroxide and its comparative characterisation with Zn–Al LDH: application on crystal violet and malachite green dye adsorption—isortherm, kinetics and Box-Behnken design

Giphin George<sup>1</sup> · Manickam Puratchiveeran Saravanakumar<sup>1</sup>

Received: 4 June 2018 / Accepted: 16 August 2018 / Published online: 28 August 2018  
© Springer-Verlag GmbH Germany, part of Springer Nature 2018, corrected publication September/2018

## Abstract

The adsorption of crystal violet (CV) and malachite green (MG) dyes using carbon-coated Zn–Al-layered double hydroxide (C–Zn–Al LDH) was investigated in this work. The characterisation of both Zn–Al LDH and C–Zn–Al LDH was performed using XRD, SEM, TEM, EDX, XPS, FTIR, BET and TGA. The results indicated that carbon particles were effectively coated on Zn–Al LDH surface. The average total pore volume and pore diameter of C–Zn–Al LDH were observed as 0.007 cc/g and 3.115 nm. The impact of parameters like initial dye concentration, pH and adsorbent dosage on the dye removal efficiency was confirmed by carrying out Box-Behnken design experiments. Langmuir isotherm was well suited for both CV and MG adsorption among other isotherm models. The adsorption capacity was maximally obtained as 129.87 and 126.58 mg/g for CV and MG respectively. Pseudo-second order fits the adsorption kinetics than any other kinetic models for both the dyes. The thermodynamic study indicates that the adsorption process of CV was exothermic, whereas for MG was endothermic. Electrostatic attraction, H-bonding,  $n$ - $\pi$  and  $\pi$ - $\pi$  interactions were mainly influenced in the adsorption process. This study concludes that C–Zn–Al LDH is an efficient adsorbent for the CV and MG dye removal from aqueous solutions.

**Keywords** Glucose · Carbon-coated Zn–Al LDH · Adsorption · Isotherms & kinetics · Box-Behnken design

## Introduction

Pollutants from industries are one of the main reasons of environmental pollution, mainly wastes produced from several dye manufacturing, dyeing, printing, textile industries, plastic and paper making industries (Mustapha et al. 2011). The emission

of these pollutants causes serious issues to the ecosystem. Especially synthetic dyes in wastewater undergo several chemical reactions and destroy aquatic species. The occurrence of dyes in water bodies declines the permeation of light and may disturb photochemical activities in aquatic organisms (Buvaneswari and Kannan 2011; Shan et al. 2015). It is also reported that many of these synthetic dyes are carcinogenic, toxic and mutagenic in nature (El Gaini et al. 2009). Hence, the elimination of dyes from textile wastewater is more significant.

Reverse osmosis, coagulation, membrane filtration, biological, chemical and photo degradation are the conventional techniques for the elimination of dyes from contaminated water (Zheng et al. 2012). Compared to these methods, the simplest technique used for the dye removal is adsorption since the process is cost-effective and very efficient and the adsorbent can be reused and the chance of producing secondary waste is very less (Yang et al. 2015). Many conventional adsorbents can be utilised to remove colour from wastewater, namely powder/granular activated carbon, fly ash, sawdust, bentonite, chitosan, sludge, rice husks and some agricultural by-products (Garg et al. 2003; Wu et al. 2013). In addition,

---

The original version of this article was revised: The original publication of this paper contains an error. The correct Figure 8 is shown in this paper.

---

Responsible editor: Tito Roberto Cadaval Jr

---

**Electronic supplementary material** The online version of this article (<https://doi.org/10.1007/s11356-018-3001-3>) contains supplementary material, which is available to authorized users.

---

✉ Manickam Puratchiveeran Saravanakumar  
saravanakumar05@gmail.com

Giphin George  
giphingeorge@gmail.com

<sup>1</sup> School of Civil and Chemical Engineering, Vellore Institute of Technology, Vellore Campus, Vellore, India

various studies were conducted for the removal of CV and MG dyes using different adsorbents. Brião et al. 2017 studied the removal of CV using mesoporous ZSM-5 zeolite as the adsorbent and obtained the maximum adsorption capacity as 141.8 mg/g. Ghazali et al. 2018 and Laskar and Kumar 2018 conducted experiments on CV dye adsorption using date palm leaves and sodium carbonate modified *Bambusa tulda* as the adsorbents and they obtained a maximum adsorption capacity of 37.73 mg/g and 20.84 mg/g respectively. Sartape et al. 2017 and Garg et al. 2004 carried out investigations on MG dye adsorption using agro-based adsorbents such as wood apple shell and *Prosopis cineraria* sawdust. In their study, the researchers obtained more than 98% removal efficiency in their tested dyes at optimum conditions. There are many advantages in using agro-based waste materials for the removal of pollutants viz., low operational costs, easy disposal of materials, moderate adsorption capacity etc. For the adsorption of CV, Mashkoo et al. 2018 obtained adsorption capacity as 131.58 mg/g when *Tectona grandis* sawdust was used as adsorbent. In addition, wood apple shell was also used Jain and Jayaram 2010 and attained 130 mg/g. For the removal of MG, Hameed and El-Khaiary 2008a utilised oil palm trunk fibre and reached up to 150 mg/g. However, the low-cost biomass material has not been a successful candidate with high adsorption capacity. A large quantity of adsorbent is essential to remove a low concentration of dyes from wastewater (Zahra et al. 2017). This is one of the main limitations for its application in the removal of pollutants. Anyway, the previous researchers (Dos Santos et al. 2011; Schwantes et al. 2016) have reported the simple and easy chemical modification techniques for enhancing the adsorption capacity of the material.

Layered double hydroxides (LDHs) contain hydrotalcite and hydrotalcite-like compounds, which possess high adsorption efficiency (Kim et al. 2004; Wang et al. 2006). LDHs are denoted by using a common formula  $[M_1-x^{2+}M_x^{3+}(\text{OH})_2]^{x+}[A^{n-}]_{x/n}m\text{H}_2\text{O}$  where the  $M^{2+}$  divalent cations ( $\text{Zn}^{2+}$ ,  $\text{Mg}^{2+}$ ,  $\text{Ca}^{2+}$ ,  $\text{Fe}^{2+}$ ,  $\text{Cu}^{2+}$ ,  $\text{Ni}^{2+}$ ,  $\text{Co}^{2+}$  etc.) are replaced to some extent by  $M^{3+}$  trivalent cations ( $\text{Fe}^{3+}$ ,  $\text{Al}^{3+}$ ,  $\text{Mn}^{3+}$ ,  $\text{Ni}^{3+}$ ,  $\text{Cr}^{3+}$ ,  $\text{Co}^{3+}$  etc.),  $A^{n-}$  is the interlayer charge balancing anion such as  $\text{CO}_3^{2-}$ ,  $\text{NO}_3^-$ ,  $\text{Cl}^-$ ,  $x$  is the  $M^{3+}$  molar fraction,  $n$  is the charge and  $m$  is the number of water molecules (Shan et al. 2015). LDHs have positive characteristics like higher surface area, large thermal stability, stable over a wide pH range, greater adsorption ability and recyclability and helps in the adsorption of pollutants from water bodies (Das et al. 2006; Del Hoyo 2007; Prasanna and Kamath 2008). LDH has a tunable structure, i.e.  $M^{2+}$  and  $M^{3+}$  cations might be interchanged or partially changed by other  $M^{n+}$  ions. Various anions are used to replace the anion that exists in the interlayer of LDH structure, anion can likewise be substituted by different anions, consequently their physicochemical properties might be changed (Ishikawa et al. 2007; Ryu et al. 2010). Moreover, LDHs can be viewed as type of materials

that can be simply synthesised in a laboratory. Using several techniques, LDH can be synthesised. The most common method is that co-precipitation method (Liu et al. 2006; Vial et al. 2008). It was proposed that the application of carbon coating onto LDH could generate plenty of hydroxyl ( $-\text{OH}$ ) groups onto the LDH surface. This permits the generation of H-bonds among dye molecules and carbon coated LDH (Zhang et al. 2014b). Meanwhile, the adsorption efficiency of the carbon-coated LDH can be significantly enhanced as the effect of supportive aids of H-bonding among dye molecules and the carbon coating.

In evaluating the role of factors influencing the adsorption process, response surface methodology has been demonstrated as a suitable statistical technique in developing the regression model. In this study, a set-batch study accomplished by Box-Behnken model was performed to assess the significant impacts of multivariate results.

The main objectives of the current study is (i) to examine the percentage dye removal for C–Zn–Al LDH towards crystal violet (CV) and malachite green (MG), (ii) to compare the material characterisation of Zn–Al LDH and C–Zn–Al LDH, (iii) to optimise the various parameters which influences adsorption such as pH, adsorbent dosage and concentration of dye, (iv) to assess the adsorption capacity and to understand the mechanism of C–Zn–Al LDH towards dyes and (v) to analyse the reusability of the dye adsorbed C–Zn–Al LDH.

## Materials and methods

### Chemicals

In this study, the chemicals utilised namely  $\text{Al}(\text{NO}_3)_3 \cdot 9\text{H}_2\text{O}$ ,  $\text{Zn}(\text{NO}_3)_2 \cdot 6\text{H}_2\text{O}$ , anhydrous  $\text{Na}_2\text{CO}_3$ ,  $\text{NaOH}$ , and glucose powder (D-glucose anhydrous) were of A.R. grade and the dyes used were crystal violet (M.W = 407.98 g/mol,  $\lambda_{\text{max}}$  = 585 nm) and malachite green (M.W = 463.50 g/mol,  $\lambda_{\text{max}}$  = 616 nm). All the chemicals were procured from SD Fine Chemicals, Mumbai.

### Methodology

#### Synthesis of Zn–Al LDH

Co-precipitation method was used for the synthesis of Zn–Al LDH. Briefly, solution A was prepared by adding 0.02 M of  $\text{Al}(\text{NO}_3)_3 \cdot 9\text{H}_2\text{O}$  and 0.04 M of  $\text{Zn}(\text{NO}_3)_2 \cdot 6\text{H}_2\text{O}$  in double distilled water. Solution B was prepared by adding 0.15 M of  $\text{NaOH}$  and 0.03 M of  $\text{Na}_2\text{CO}_3$  in double distilled water (Crespo et al. 1997). Further, solution B was added dropwise into solution A. The best homogeneity of the solution was obtained by placing the beaker over a magnetic stirrer with a fixed speed of 750 rpm for 24 h. The reaction was performed

at the ambient condition with pH was preserved within 11 and 12. The mixture was centrifuged at 4500 rpm for 5 min and recovered a white-jelly type substance. The recovered substance was washed with double distilled water and dried for 24 h at 65 °C (Marangoni et al. 2000).

### Synthesis of C–Zn–Al LDH

Glucose solution was made by dissolving 6 g of glucose anhydrous in 100 mL of double distilled water. Ten grams of synthesised slurry LDH was mixed with 100 mL of prepared glucose solution and kept in a magnetic stirrer. Water was vaporised during stirring at 100 °C for 120 min. Glucose-encapsulated LDH was dried using a bio-chem hot air oven at 50 °C for 24 h. The dried compound was placed in the furnace at 350 °C for 15 mins. The recovered product was brown in colour and conserved in a desiccator for future application.

### Adsorbent characterisation

LDHs were characterised using transmission electron microscopy (TEM-FEI Tecnai G2 T20 S-Twin) and scanning electron microscopy (SEM-Carl Zeiss; EVO 18) to analyse the surface morphology and size of the synthesised material. The Brunauer-Emmett-Teller (BET) analysis was performed with the help of Quantachrome Nova: 1000e analyser to determine the surface area of LDH. The phase identification was observed using X-ray diffraction (XRD; Bruker, D8-Advance). X-ray photoelectron spectroscopy (XPS) by Kratos Analytical, Axis Ultra was used to analyse the elemental composition of the adsorbent. The functional groups were identified using fourier transform infrared spectrometer (FTIR, Model: IR Affinity-1, Shimadzu). Thermogravimetric analysis (TGA) of adsorbent were analysed by TA instruments SDT-Q600. Electrochemical methods were extensively used to characterise various materials like activated carbon (Álvarez-Merino et al. 2008), bio-char (Zhao and Lang 2018) and nanomaterials (Jha et al. 2018). The values of isoelectric point (IEP) indicates only the outer surface charges of the material whereas the point of zero charge convey both the inner and outer charge of the material (Menendez et al. 1995). In this study, point of zero charge was performed to determine the charge of C–Zn–Al LDH. The detailed methodology is given in the following section.

**Point of zero charge (pHpzc)** A set of 6 batch experiments with different pH values was used to evaluate the point of zero charge of C–Zn–Al LDH. The  $\text{pH}_{\text{initial}}$  values were adjusted in the range of 2 to 10 by adding  $\text{H}_2\text{SO}_4$  or NaOH to 20 mL of double distilled water. Then, 0.3 g of C–Zn–Al LDH was added to each solution. Later, the solutions were kept in an

orbital shaker for 24 h at room temperature, filtered using Whatman #41 filter paper and the  $\text{pH}_{\text{final}}$  of the solution was measured.  $\Delta\text{pH}$  was obtained by finding the difference between  $\text{pH}_{\text{initial}}$  and  $\text{pH}_{\text{final}}$  for each solution. The point of zero charge (pHpzc) was determined from the plot  $\Delta\text{pH}$  vs  $\text{pH}_{\text{initial}}$  (Lee et al. 2011; Ealias and Saravanakumar 2018).

### Dye stock solution preparation

One gram of CV and MG was deliquesced separately in 1 L of double distilled water for the preparation of the stock solution of respective dyes. This prepared stock was further diluted to wanted concentrations for adsorption studies. The initial and final concentrations of CV and MG were analysed using UV–visible spectrophotometer (Spectroquant, Pharo 300).

### Adsorption procedure

Box-Behnken experiments were performed by adding different dosages (0.05–0.15 g/100 mL) of C–Zn–Al LDH with 100 mL of the dye solution at 50–100 mg/L concentration in a conical flask at room temperature as shown in Table S2. The pH of the solution was changed from 5 to 9 for CV and 3 to 6 for MG using 0.1 N of  $\text{H}_2\text{SO}_4$  and NaOH solution. At the desired time intervals, the sample was collected and filtered using Whatman #42 filter paper. Isotherms and kinetics were studied using the obtained results.

The amount of dye adsorbed onto Zn–Al LDH/C–Zn–Al LDH and percentage dye removal were calculated with Eqs. 1 and 2

$$q_e = (C_o - C_e) \times \frac{V}{m} \quad (1)$$

$$\text{Percentage dye removal} = \frac{C_o - C_e}{C_o} \times 100 \quad (2)$$

the initial and equilibrium concentrations of dye (mg/L) were denoted by  $C_o$  and  $C_e$  respectively,  $m$  is the mass of the adsorbent (g),  $V$  is the volume of dye solution and  $q_e$  is the amount of dye adsorbed at equilibrium in mg/g (Sharifpour et al. 2017).

### Recycling experiments

After the adsorption experiments, the used C–Zn–Al LDH was isolated by filtration and dried. Then, the dye adsorbed C–Zn–Al LDH was washed with 0.01 N NaOH solution and recovered using filtration and kept for drying. Then, the regenerated adsorbents go through the next adsorption cycle. The recycling experiments of both CV and MG dyes were conducted for five consecutive cycles.

## Results and discussion

### Adsorbent characterisation

The XRD plot of Zn–Al LDH was represented in Fig. 1b. It was perceived that at low  $2\theta$  values a sequence of peaks appeared as sharp intense symmetric lines and at higher  $2\theta$  values, clear reflections were observed representing the basal planes of hydroxylated-like LDH particles (Wang et al. 2008). The diffraction peaks at  $11.77^\circ$ ,  $23.66^\circ$ ,  $34.02^\circ$ ,  $34.76^\circ$ ,  $39.40^\circ$ ,  $44.20^\circ$ ,  $47.01^\circ$ ,  $60.48^\circ$  and  $61.85^\circ$  are allocated to the planes (003), (006), (101), (012), (015), (107), (018), (110) and (113) detected from XRD pattern (Fig. 1b), representing the high crystallinity of LDH, that agree with SAED pattern, representing the presence of zinc aluminium carbonate hydroxide hydrate (JCPDS No. #00-048-1024). Strong peaks at (003) and (006) planes were detected and the angle of (003) plane shown large spacing among interlayers (Yan et al. 2015). The interlayer d-spacing are of 0.752 nm at  $d_{003}$  and 0.376 nm at  $d_{006}$  respectively. The  $d_{003}$  was double as much as  $d_{006}$ , signifying a good layer structure (Evans and Slade 2006). The planes of (015), (012) and (110) were represented that the hexagonal lattice with rhombohedral 3R symmetry (Jenisha et al. 2016). After coating with the carbon, the diffraction spectrum of C–Zn–Al LDH (Fig. 1a) indicates a reflection characteristic of amorphous carbon.

SEM analysis was utilised to investigate the particle size and morphology of the samples. Besides the textural difference, microstructure was also observed. Partial aggregation was analysed through the images of Zn–Al LDH and C–Zn–Al LDH. The morphology of Zn–Al LDH crystals was observed to have a hexagonal platelet structure with smooth texture as shown in Fig. S1(a). Hence, C–Zn–Al LDH shown pores with irregular surfaces of dissimilar sizes and shapes as shown in Fig. S1(b). The average size of Zn–Al LDH was observed to be in the range of 200–400 nm whereas the size of the C–Zn–Al LDH was not identified since agglomeration of the particle has taken place.

TEM images portray that the Zn–Al LDH have a hexagonal plate-like structure with  $90 \pm 20$  nm as side length as represented in Fig. 2b. Figure 2a describes the structure of Zn–Al LDHs as an octahedral unit. The micrometre-sized inorganic sheets are formed by sharing the edges of  $Zn^{2+}$  or  $Al^{3+}$  (sixfold coordinated to  $OH^-$ ) octahedral units. A complete positive charge was generated in the brucite-type layers due to the higher charge of  $Al^{3+}$  and, also, balanced use of interlayer intercalation of anions (Cho et al. 2009). The SAED (selected-area electron diffraction) image (Fig. 2d) shows patterns with ring shape having brighter spots, indicating the Zn–Al LDH as crystalline with planes (101), (012), (110) and (107). The average gap between hydroxyl groups (lattice spacing) was about 0.241 nm with (104) plane as shown in Fig. 2c. The results of SAED were matching with the XRD spectrum.

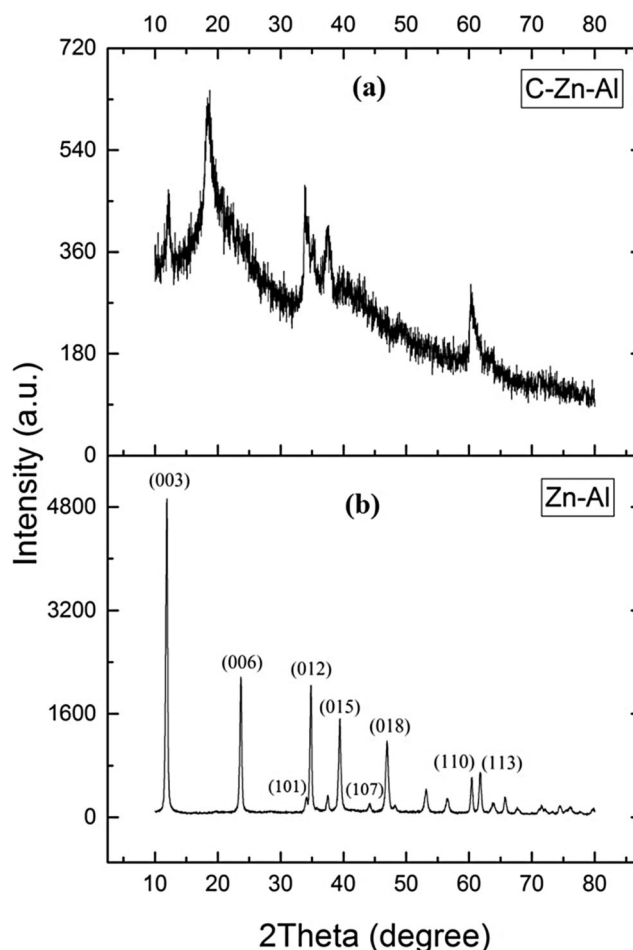
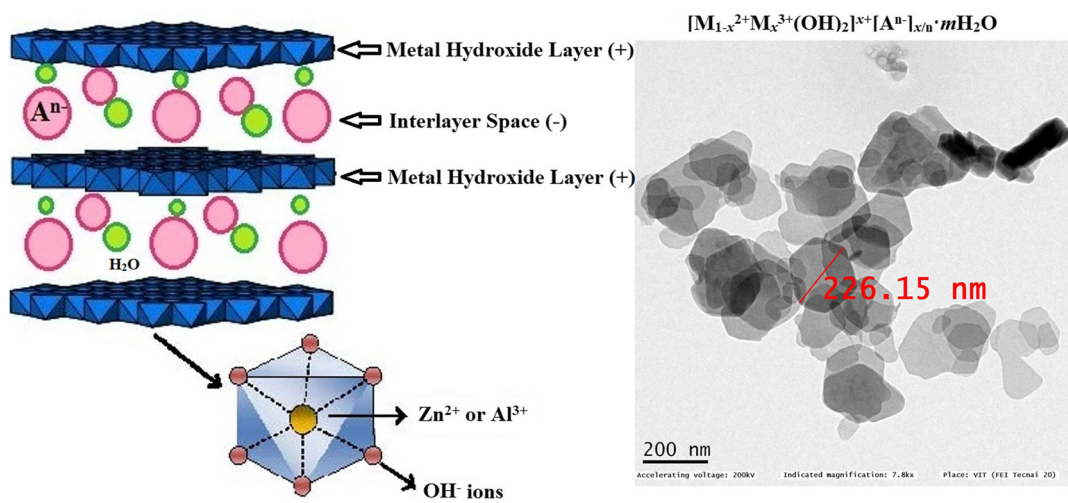


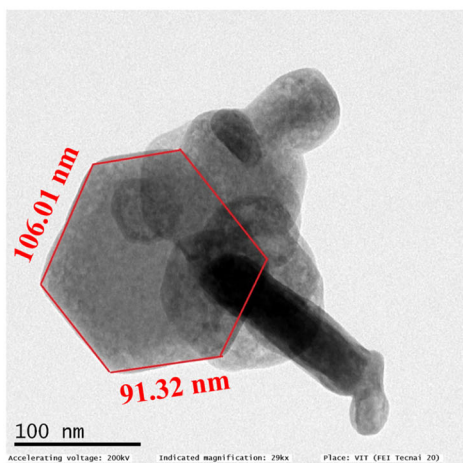
Fig. 1 XRD Spectrum of (a) C–Zn–Al LDH and (b) Zn–Al LDH

Figure S2(a) represents the EDX of Zn–Al LDH. As shown in Fig. 3a, b C–Zn–Al hexagonal plates were covered with carbon coating and also it indicates that the hexagonal shape of Zn–Al LDH was not disturbed during its synthesising period. SAED of C–Zn–Al was getting amorphous because crystalline Zn–Al particles were covered with carbon particles as shown in Fig. 3c. Moreover, in SAED a mist diffraction ring and no observable crystal inter-fringe is detected which confirms that the product is amorphous when it is synthesised at  $350^\circ\text{C}$  (Zhang et al. 2013). And, this result is in good conformation with those of XRD patterns and TEM. Figure S2(b) represents the EDX spectra of C–Zn–Al LDH which designate that the carbon content was more in C–Zn–Al LDH than Zn–Al LDH and prove that the carbon is effectively coated over the normal Zn–Al LDH. Also, the atomic and weight percentage of Zn, Al, O and C for both LDHs is shown in Table S1. Further, the average size of the particle was observed to be 200 nm which confirms with SEM analysis.

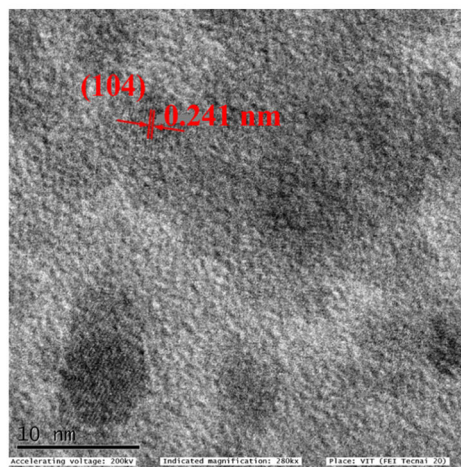
The surface chemical configuration of Zn–Al LDH and C–Zn–Al LDH was determined using XPS. The wide spectrum (Fig. 4) shows that core levels of Zn, Al, C and O were observed. The Auger parameter of Zn value is represented by Zn



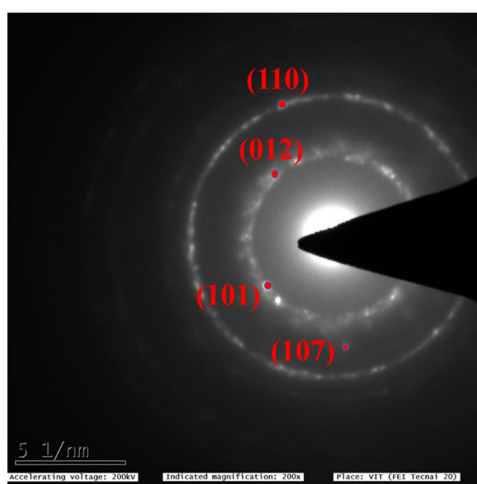
(a)



(b)



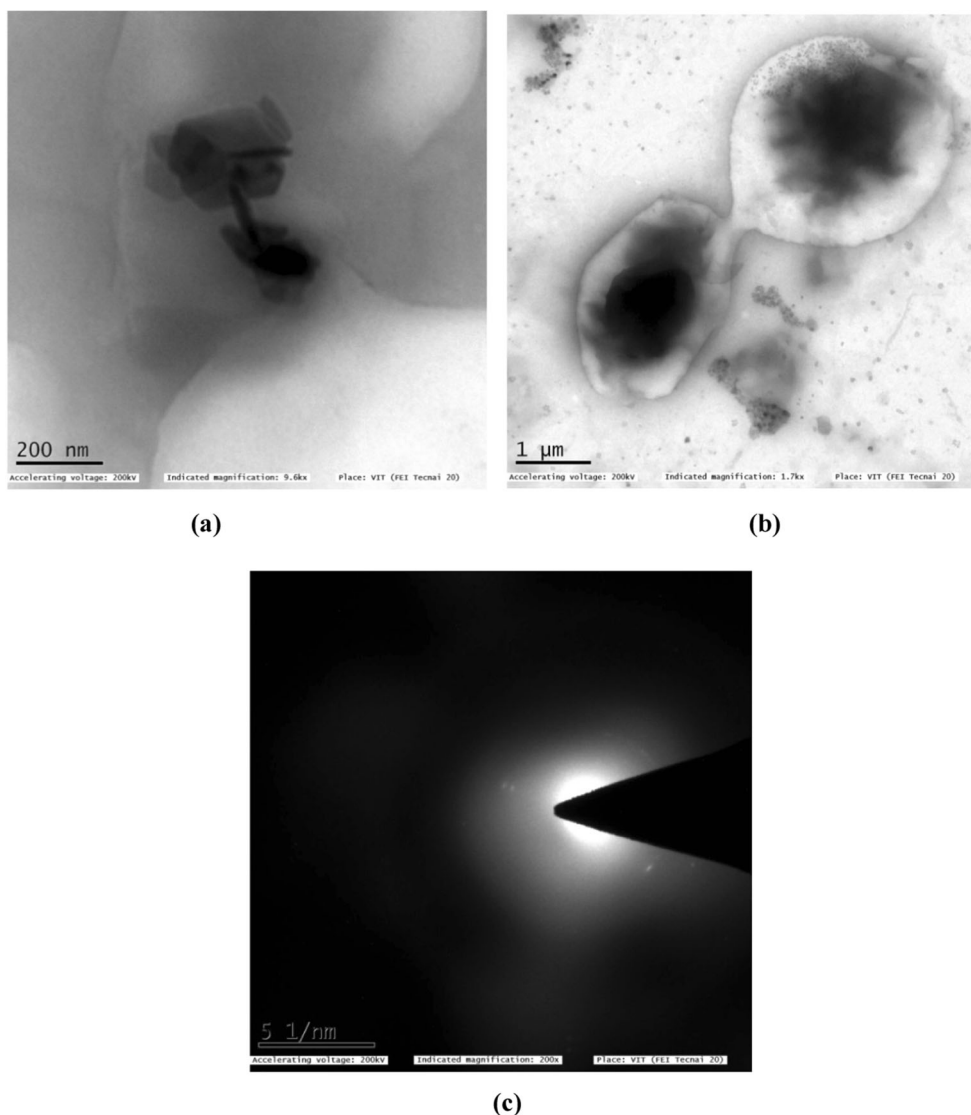
(c)



(d)

**Fig. 2** (a) TEM images of Zn–Al LDH: schematic diagram of the structure of the Zn–Al LDH; (b) high-magnified images of a Zn–Al LDH; (c) interfringe distance of Zn–Al LDH; (d) SAED image of Zn–Al LDH

**Fig. 3** (a), (b) TEM images of C–Zn–Al LDH at different magnifications; (c) SAED image of C–Zn–Al LDH

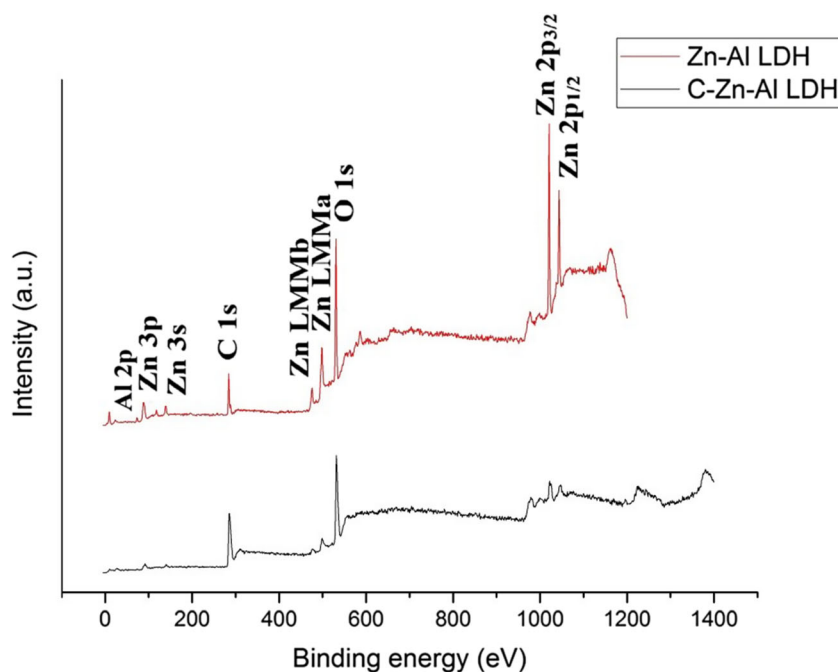


LMMa and Zn LMMb (495.3 and 474.2 eV) is in which confirms the formation of ZnO (Gaddam et al. 2015). Zn 2p core level binding energies of Zn–Al LDH have two fitting peaks sited at 1043.8 eV and 1020.69 eV and, which is ascribed to Zn 2p<sub>1/2</sub> and Zn 2p<sub>3/2</sub> respectively (Fig. 5a). These outcomes portray that the valence state of zinc at the surface of Zn–Al LDH is + 2 (Lu et al. 2017). But, there was a small shift in the peak for the LDH coated with carbon as shown in Fig. 5a\* (1026.23 and 1049.18 eV). The Al 2p spectrum detects at 73.3 eV in Fig. 5b. The C1s high-resolution spectra displayed three deconvoluted peaks located at 288.17, 285.7 and 284.3 eV that was conveyed with C=O, C–O and C–C respectively (Chen et al. 2016) shown in Fig. 5c. All these peaks were observed in C–Zn–Al LDH also, along with an extra peak of O=C=O at 289.75 eV (Fig. 5c\*). The existence of O–H, O=C and O–C are assured by O 1s spectrum (Fig. 5d) at 530.6, 531.2 and 533.6 eV respectively for Zn–Al LDH. Similar peaks were observed in C–Zn–Al LDH (Fig.

5d\*). From Fig. 4 it can be observed that the intensity of Zn and Al peaks in Zn–Al LDH was reduced after the LDH was coated with carbon.

The FTIR spectra (Fig. 6) show the Zn–Al LDH, C–Zn–Al LDH and after adsorption of crystal violet and malachite green dyes. As shown in Fig. 6a, the band presented at 3377.36 cm<sup>-1</sup> corresponds to O–H due to absorption of water, interlayer water and M–OH (Zhao et al. 2016). The presence of shoulder peak at 2970.38 cm<sup>-1</sup> is attributable to CO<sub>3</sub><sup>2-</sup>–H<sub>2</sub>O indicates the existence of a bond between the CO<sub>3</sub><sup>2-</sup> and water molecule hydrogen. The bond at 1355.96 cm<sup>-1</sup> could be ascribed to the symmetric/asymmetric stretching of interlayer carbonate ion (Yang et al. 2014). In addition, the peaks at 767.67 and 549.71 cm<sup>-1</sup> depict the vibrational manner of Al–OH and Zn–OH at the crystal lattice layer (Zahra et al. 2017). Moreover, the significant peak at 1355.96 and the other peak at 1630 cm<sup>-1</sup> could be allocated to C–O asymmetric stretching due to carbonate ion. In Fig. 6b, the presence of peaks at

**Fig. 4** XPS wide spectra of Zn–Al LDH and C–Zn–Al LDH



1585.49 (C=C), 1369.46 (C–H), 1745.58 (C=O) and 1028.06  $\text{cm}^{-1}$  (C–O) indicates the possibility of carbon encapsulation over Zn–Al LDH (Cho et al. 2016). The functional group like O–H bonds and C=O of COOH involved to the C–Zn Al LDH by peaks at 1745.58 and 3294.42  $\text{cm}^{-1}$  respectively. Figure 6c shows the CV dye adsorbed C–Zn Al LDH with significant changes in the functional groups in comparison with the unloaded adsorbent. Specifically, the peak intensity at 1028.06  $\text{cm}^{-1}$  was decreased in the CV loaded adsorbent. This indicates the significant role of C–O in the adsorption of CV onto C–Zn–Al LDH. The slight shift and decrease in intensity were observed at 1361.74  $\text{cm}^{-1}$  which depicts the involvement of C–H functional group in the adsorption

process. The involvement of the functional groups like C=C and C=O was found with the decrease in intensity and minor change in the peaks. Like CV, similar results were observed in MG dye adsorbed C–Zn Al LDH. The alterations observed after adsorption of dyes in the functional groups indicate the existence of hydrogen bonding, electrostatic attraction and  $n-\pi$  interaction between the cationic dye molecules and C–Zn–Al LDH. The details of the above-mentioned interactions are discussed in section “Adsorption isotherm”.

The pore-size distribution and surface area measurement of Zn–Al LDH and C–Zn–Al LDH are represented in Fig. 7. The results revealed that the specific surface area of the Zn–Al LDH and C–Zn–Al LDH was 38.267 and 4.554  $\text{m}^2/\text{g}$  having

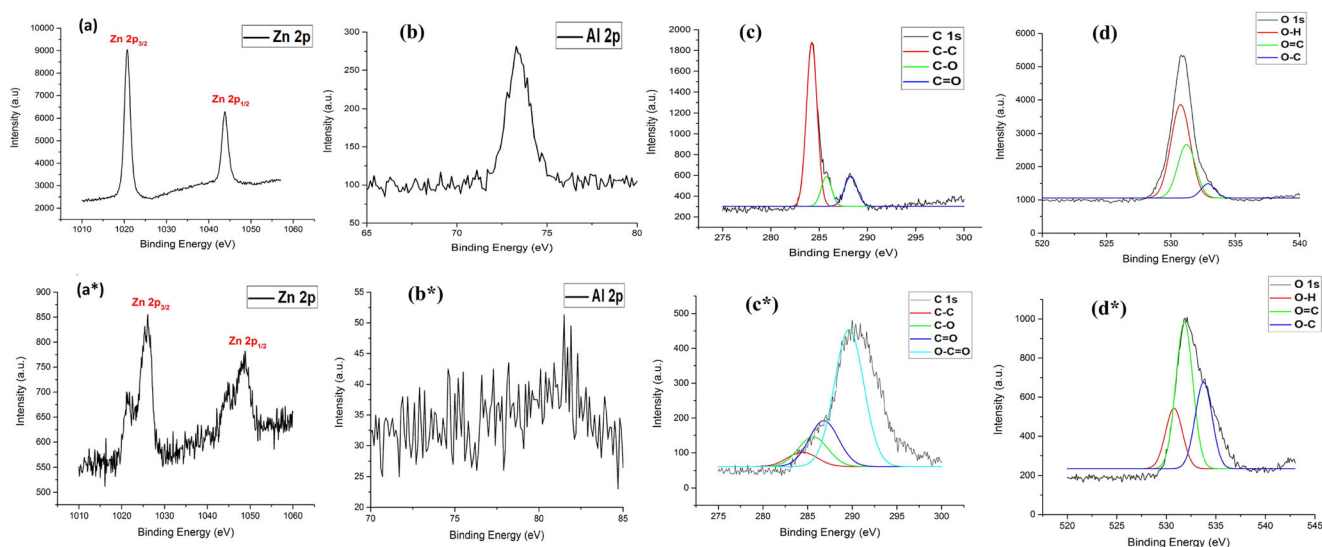
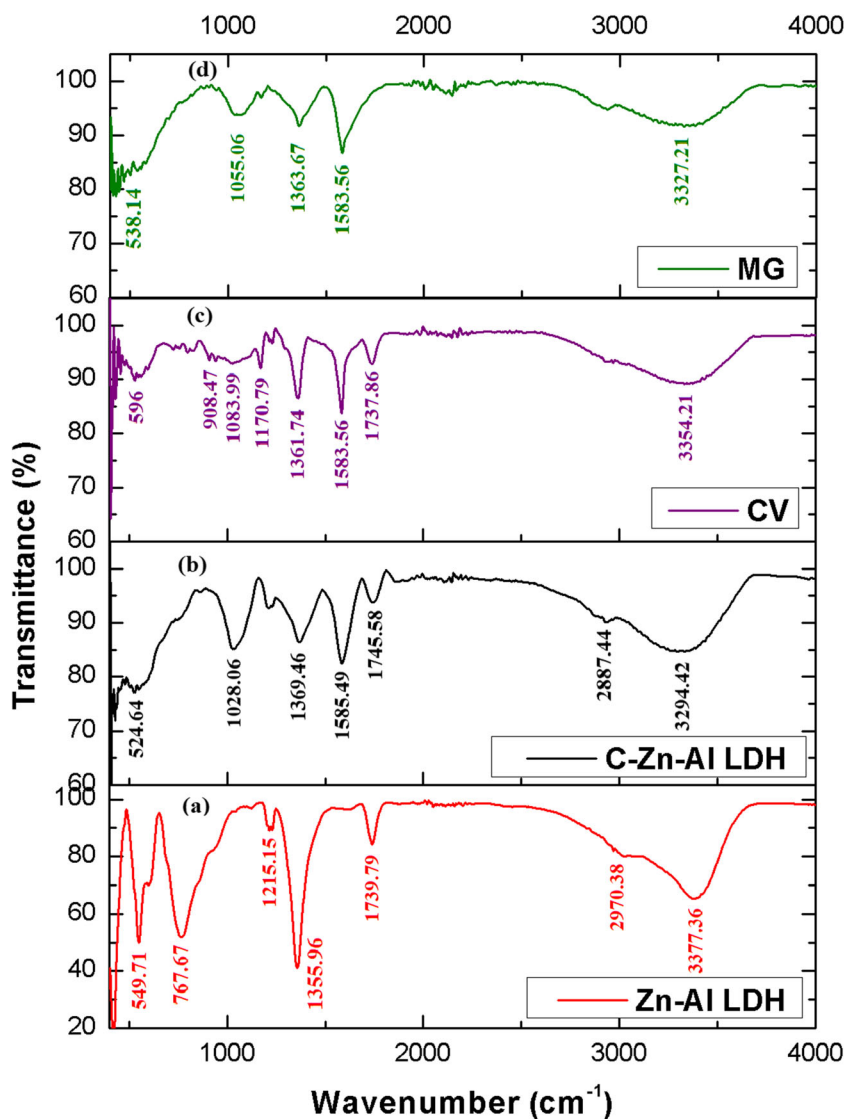


**Fig. 5** XPS spectra of Zn–Al LDH and C–Zn–Al LDH: peaks corresponding to (a,a\*) Zn 2p, (b,b\*) Al 2p, (c,c\*) C 1s and (d,d\*) O 1s

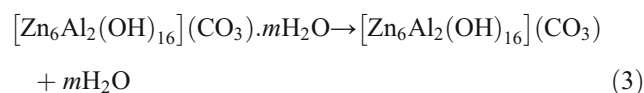
**Fig. 6** FTIR spectra of (a) Zn–Al LDH, (b) C–Zn–Al LDH (c) after adsorption of CV, (d) after adsorption of MG



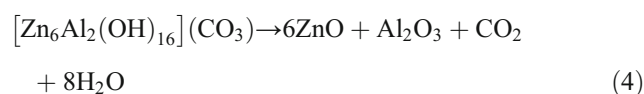
a total pore volume of 0.082 and 0.007 cc/g respectively (Fig. 7a). The pore diameter was determined using Barrett-Joyner-Halenda (BJH) analysis and it was found to be 1.486 and 3.115 nm. Figure 7b visibly demonstrates that in the mesoporous range (2–50 nm diameters) greater than 90% of the pores were observed and in the microporous range (<2 nm) less than 10% pores were detected. The adsorption capacity of C–Zn–Al LDH is very strong since the pore diameter was higher than the molecular size of CV (1.65 × 1.50 nm (Iwasaki et al. 2000)) and MG (1.1 × 1.2 nm (Issa et al. 2014)) which helps in pore diffusion.

Thermal stability of synthesised materials with regard to weight loss was analysed by thermogravimetric experiments. TGA curve of Zn–Al LDH is presented in Fig. S3(a). Three weight-loss stages were perceived as the temperature was enhanced from 30 to 800 °C. The first weight loss step of 13.35% from temperature 30 to 191 °C resembles the removal of both the interlayer adsorbed water and surface adsorbed

water (Huang et al. 2015) that can be ascribed by the given equation:



The second weight-loss step of 10.28% from temperature 191 to 325 °C indicates the dehydration of Zn–Al LDH (brucite-like layers). The third weight loss step of 5.776% in a range of temperature varying from 325 to 791 °C can be owing to the disintegration of OH<sup>-</sup> and carbonate ions into the LDH layers (Huang et al. 2015) which can be described by the given equation:





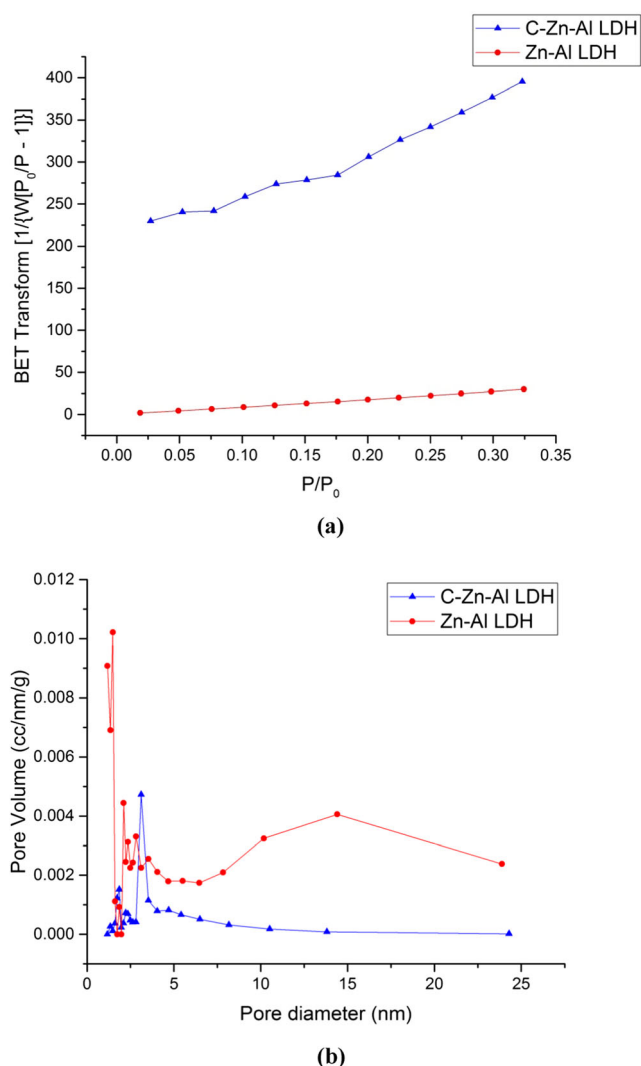


**Fig. 7** (a) Pore size distribution of C–Zn–Al LDH and Zn–Al LDH (b) Surface area measurement of C–Zn–Al LDH and Zn–Al LDH

It was observed that the carbothermal reduction peak was around 230 °C (Fig. S3(b)). During this carbonisation process, it is proposed that the metal alloys and metals might have formed. It was observed that the completion of combustion reaction around 525 °C due to the volatilisation of the glucose molecules. In regard to the TGA curves, the carbon content weight percentage was estimated around 50%.

## Adsorption isotherm

Adsorption isotherm specifies how the adsorbent particle works with adsorbate molecules and achieves equilibrium. The equilibrium isotherm profile is drawn between  $q_e$  and  $C_e$  (Fig. S4). The study on the isotherm model was accomplished with the help of five linearised models such as Langmuir, Freundlich, Temkin, Redlich–Peterson and Sips model to fit the parameters attained from various experiments. The correlation coefficient ( $R^2$ ) and parameters for the five

different models are shown in Table 1. The higher correlation coefficient ( $R^2 = 0.976$  &  $0.923$ ) suggests that both CV and MG adsorption were more suitable to Langmuir isotherm. A graph between  $1/q_e$  vs  $1/C_e$  was plotted and  $Q_m, K_L$  were the constants gained from the intercept and slope as shown in Fig. S5(a). Langmuir model predicts that maximum adsorption capacity ( $Q_m$ ) of C–Zn–Al LDH for CV was 129.87 mg/g and 126.58 mg/g for MG. Another parameter  $K_L$  denotes the relationship between energy of adsorption and adsorption–desorption rate constant and the values of 0.291 for CV and 0.05 L/mg for MG. The values of dimensionless constants  $R_L$  were 0.043 (CV) and 0.207 (MG) which satisfies that the Langmuir isotherm is favourable. A plot of  $\log q_e$  vs  $\log C_e$  shows a straight line with intercept ( $\log K_f$ ) and slope ( $1/n$ ) indicates Freundlich isotherm (Fig. S5b). The expected values of parameters  $K_f$  and  $n$  are 4.89 mg/g and 2.56 for CV and 3.05 mg/g and 1.9 for MG respectively. The slope ( $1/n$ ) value is getting in the range 0–1 is used to find the surface heterogeneity. If the slope value is nearer to zero, heterogeneity is high (Foo and Hameed 2010). The Temkin coefficients  $B$  and  $A_T$  are the heat of adsorption and maximum binding energy. These were assessed from the slope and intercept of Fig. S5(c). The values of  $B$  were 30.446 J/mol and 32.412 J/mol, while the values of  $A_T$  were 2.419 L/g and 0.368 L/g for CV and MG respectively. In Redlich–Peterson isotherm model, a graph plotted between  $\ln(K_R \frac{C_e}{q_e} - 1)$  vs  $\ln C_e$  shows a straight line with an intercept  $\ln a_R$  and slope  $b_R$  as shown in Fig. S6(a).  $K_R$  is the Redlich–Peterson adsorption capacity constant evaluated via trial and error method. The parameters were calculated and presented in Table 1. When  $b_R = 1$ , the Redlich–Peterson equation becomes more suitable to the Langmuir isotherm model and when  $b_R = 0$ , it is closer to the Freundlich isotherm model (Konicki et al. 2017). A plot of  $\ln(\frac{K_s}{q_e})$  vs  $\ln C_e$  shows a straight line with an intercept  $\ln a_s$  and slope  $-\beta_s$  represents Sips isotherm as shown in Fig. S6(b). The Sips isotherm constants  $K_s$ ,  $a_s$  and model exponent ( $\beta_s$ ) were also presented in Table 1. The obtained value of  $R^2$  depicts that the Langmuir model was more suitable for the adsorption of CV and MG on to C–Zn–Al LDH. This observation concludes that a monolayer homogeneous adsorption (Kim et al. 2015) occurs throughout the elimination of CV and MG on the active spots available in C–Zn–Al LDH.

## Adsorption kinetics

The kinetic profile of both the dyes drawn between  $q_t$  and  $t$  is presented in Fig. S7. The adsorption rate for the CV and MG removal was examined with kinetic models such as pseudo-first order, pseudo-second order, Elovich and Weber–Morris intraparticle diffusion. The linear fitness of the  $\log(q_e - q_t)$  vs  $t$ ,  $t/q_t$  vs  $t$ ,  $q_t$  vs  $\ln t$  and  $q_t$  vs  $t^{1/2}$  was estimated and results are

**Table 1** Parameters and the correlation coefficients of isotherm models for the adsorption of CV and MG onto C–Zn–Al LDH

Two parameter models										Three parameter models						
Langmuir				Freundlich			Temkin			Redlich-Peterson				Sips		
$Q_m$ (mg/g)	$K_L$ (L/mg)	$R_L$	$R^2$	$K_f$ (mg/g)	n	$R^2$	$A_T$ (L/g)	B (J/mol)	$R^2$	$K_R$ (L/g)	$a_R$ (1/mg)	$b_R$	$R^2$	$\beta_s$	$a_s$ (L/mg)	$R^2$
Crystal violet																
129.87	0.291	0.043	0.976	4.89	2.56	0.967	2.419	30.446	0.963	110	2.103	0.697	0.971	0.390	3.101	0.9676
Malachite green																
126.58	0.05	0.207	0.923	3.05	1.9	0.909	0.368	32.412	0.881	60	4.007	0.501	0.892	0.5261	6.900	0.9097

presented in Fig. S8(a–d). Based on the data given in Table 2, the correlation coefficient ( $R^2$ ) values attained from second-order kinetics were 0.998 for CV and 0.996 for MG respectively. The value of  $(q_e)_{cal}$  attained from the pseudo-first order kinetic equation was considerably varied from  $(q_e)_{exp}$ . Coefficient of regression ( $R^2$ ) value obtained from second-order kinetics was greater than further three kinetics models depicting that this kinetic model gives a better correlation with respect to the experimental data. From the Table 2 it is visible that there was no much deviation between calculated and experimental adsorption capacities. Also, the  $R^2$  values were obtained to be nearer to 1 than any other kinetic models. Pseudo-second order rate constant ( $k_2$ ) is getting low for both the dyes which indicate that the adsorption process is rapid. It indicates that in a single site two molecules can be adsorbed, or a single molecule can interact with two adsorption sites (Hemmati et al. 2016). This finding shows that the rate of adsorption is much dependent on the accessibility of active spots proposing a chemisorption process (Chakraborty and Nagarajan 2015).

Figure S8(d) shows the intra-particle diffusion model of CV and MG. The plot represents the two stages of the adsorption process. The first stage depicts that best fit is not passing through the origin demonstrating the resistance of the boundary layer in the previous stage of adsorption (Abd El-Latif et al. 2010). From the table, it was observed that there was a less intercept value and a sharp rise in the first stage for both the dyes. The second stage shows a straight fit, which portrays the variation in the mass transfer rate in both stages of adsorption (Elmorsi 2011). The results showed that not only the pore diffusion but also bulk- and intra-particle diffusions perform a significant role in both stages of adsorption. The  $R_a^2$ ,  $C_a$  and  $k_{ia}$  are the correlation factor, intercept and slope of first sharper portion while  $R_b^2$ ,  $C_b$  and  $k_{ib}$  denotes the linear portion in the second phase. Meanwhile, the  $k_{ia}$  values are higher than the perceived values of  $k_{ib}$ , designates that the intraparticle diffusion model mostly controls the uptake of dyes on to the adsorbents. The intercept value was smaller in the first phase than the second phase portraying the effect of boundary layer.

### RSM optimisation for dye adsorption

RSM was utilised to analyse the influence of variables namely pH (A), C–Zn–Al LDH dosage (B) and initial dye concentration (C) on the percentage removal of CV and MG dyes using Box-Behnken design (BBD). The adsorption capacity of C–Zn–Al LDH with coded values (–1, 0, +1) containing three different levels was shown in Table S2 ensued in 17 experiments, and in Table S3 and S4 their responses are represented. The predicted percentage removal response for CV and MG dyes were attained by Eqs. (5) and (6).

$$R_1 = +94.84 + 2.66 \times A + 7.63 \times B - 3.86 \times C + 1.04 \times AB + 1.30 \times AC + 4.81 \times BC - 2.06 \times A^2 - 7.12 \times B^2 - 0.76 \times C^2 \tag{5}$$

$$R_2 = +73.08 + 8.39 \times A + 6.50 \times B - 3.91 \times C + 4.89 \times AB - 0.68 \times AC - 0.51 \times BC - 2.08 \times A^2 - 6.77 \times B^2 - 4.67 \times C^2 \tag{6}$$

where  $R_1$  and  $R_2$  were the response (dye removal efficiency) of CV and MG respectively. Fisher’s statistical test used for the statistical testing of the model was carried out with analysis of variance (ANOVA) as shown in Table S5 and Table S6 for CV and MG respectively. The Model  $F$ -value of CV and MG are 54.66 and 17.18 which denotes the model is significant. There is only 0.01 and 0.06% chance for CV and MG that an  $F$ -value this large may happen because of noise. The values of “Prob > F” less than 0.05 denote that the model is significant (Ealias et al. 2016). In the case of crystal violet and malachite green, the terms A, B, C, BC,  $A^2$ ,  $B^2$  and A, B, C, AB,  $B^2$ ,  $C^2$  are significant respectively. The values higher than 0.10 denote that the model parameters are not significant.

The predicted and measured dye removal efficiencies were dispersed close to straight line, since the measured and predicted removal efficiencies were the same. This shows that the mathematical model is capable to predict the adsorption of dye

**Table 2** Adsorption kinetic models and parameters for removal of CV and MG dye onto C–Zn–Al LDH adsorbent

Dye (mg/L)	$(q_e)_{exp}$ (mg/g)	Pseudo-first order		Pseudo-second order		Elovich		Intra-particle diffusion					
		$(q_e)_{cal}$ (mg/g)	$k_1$ ( $min^{-1}$ )	$R^2$	$(q_e)_{cal}$ (mg/g)	$k_2$ (g/mg/min)	$R^2$	$\alpha$ (mg/g/min)	$\beta$ (g/mg)	$R^2$	$k_{ia}, k_{ib}$ (mg/g/min <sup>1/2</sup> )	$C_a, C_b$ (mg/g)	$R_a^2, R_b^2$
Crystal violet													
75	117.645	53.09	0.0096	0.933	106.38	0.0008	0.998	58.50	0.0612	0.974	6.851, 2.897	37.47, 66.64	0.953, 0.9309
Malachite green													
75	87.03	63.76	0.029	0.982	99.009	0.0005	0.996	14.3	0.05	0.974	7.974, 1.650	14.64, 67	0.995, 0.9042

as shown in Fig. S9. The desirability profile drawn from the predicted values of adsorption for both the dyes were shown in Fig. S10(a) and (b). It displays that the desirability is nearer to one representing the best favoured for optimal performance. The maximum percentage removal of CV and MG were 97.87 and 85.67%, and the minimum was 70.87 and 52.58% using Box-Behnken design experiments. From desirability profile, the optimum conditions for the effective elimination of CV and MG were observed at pH 9 and 6, 0.15 g/100 mL of C–Zn–Al LDH dosage and 75 mg/L of the initial dye concentration respectively.

**Influence of independent parameters on adsorption**

**Influence of pH**

For observing the stability of the dyes, UV visible spectral analysis was carried out at different pH values for CV and MG. Fig. S11 shows the spectrum of CV and MG at 75 mg/L as initial concentration. The main peak was observed at their respective  $\lambda_{max}$  values 585 nm for CV and 616 nm for MG. The results show that the spectrum was not affected by the changes in the pH. For CV, the maximum peak persists in the pH range of 5 to 9 whereas for MG 3 to 6. Either change in colour or disappearance of colour was observed beyond the tested pH values for both the dyes. Similar studies were observed by Cheriaa et al. 2012; Adel and El-Zahhar 2016. Hence, all the dye adsorption tests were performed in the stable pH range. The experimental results (Fig. S12(a–d)) denote that as pH increases the removal efficiency of CV and MG were increased. The minimum dye removal for CV (75.54%) and MG (52.58) was perceived at pH 5 and 3 respectively whereas the maximum dye removal for CV (97.87) and MG (85.67) was observed at pH 9 and 6.

In the case of CV adsorption, at acidic pH, the amount of active spots with a positive charge is higher when compared to sites having negatively charged. Further, the carboxylic groups present in CV gets protonated and a greater positive charge is possessed at acidic pH (Garg et al. 2003). Therefore, a decrease in the solution pH (an increase of H<sup>+</sup> ion) increased the electrostatic repulsion among the dye molecules having positive charge and adsorbent sites, ensuing in the reduction in adsorption ability of CV. On other hands, carbonyl and hydroxyl functional groups can act as biosorbing agents or sites having negative charge (Sartape et al. 2017). At alkaline pH, the adsorbent surface sites have a negative charge that favours the removal of positive charge cationic dyes because of electrostatic attraction. Consequently the adsorption of CV onto the adsorbent particles enhanced with an enhancement in pH values (Xiangliang Pan 2009; Sartape et al. 2017).

In the case of MG adsorption as pH increases, the removal efficiency also increases. This behaviour should be ascribed to, firstly, electrostatic repulsion occurs among C–Zn–Al

LDH and MG due to the same positive charges; secondly, the extra H<sup>+</sup> ions present in the solution having acidic pH will compete with dyes having positive charge to reach the adsorbent surface; finally, the C–Zn–Al LDH will decompose in acid pH, tends to decrease the active adsorption spots on the surface of adsorbent (Zhang et al. 2017). Whereas at pH 6, MG is observed in its protonated form as MG<sup>+</sup> and C–Zn–Al LDH holds negative charges on its surface (pHpzc = 5.85). The mechanism presented in the adsorption process might be deliberated as the electrostatic attraction among the COO – group (Tran et al. 2017b) and the positively charged dye molecules. Moreover, CV and MG adsorption from pH deliberates that, not only electrostatic attraction but also the functional groups be present on the C–Zn–Al LDH surface were also predicted to inspire the adsorption process in advance and is deliberated in section “Adsorption mechanism”.

**Influence of adsorbent dosage**

The influence of dosage on adsorption of CV and MG dyes were analysed by changing dosages from 0.05–0.15 g to the 100 mL dye solution (Fig. S12(a), (b), (e) and (f)). In the case of CV adsorption, the removal efficiency is 80.41% at 0.05 g and then increases up to 98.07% and again decreases to 96.9% at 0.15 g as shown in Fig. S12(a). In the case of MG adsorption, the effect of C–Zn–Al dosage and pH is examined and represented in Fig. S12(b). The removal efficiency is 62.06% at 0.05 g and then increases up to 84.16% at 0.15 g. The improvement in the percentage removal with an enhancement in mass of adsorbent is owing to its large specific surface area and sufficient reactive surface centre. The rate of adsorption considerably increased due to the accessibility of more active adsorption spots and an increase in surface area (Hafshejanian et al. 2016). The percentage of dye removal gradually reduced due to deficiency of responsive spots and a lesser dye molecule ratio to evacuate spot at lower amount of adsorbent dosage.

**Influence of initial dye concentration**

The influence of the initial concentration of dye on the percentage reduction of CV and MG dyes was studied by changing the concentration from 50 to 100 mg/L of dye solution (Fig. S12(c–f)). In the case of adsorption of CV, it can be seen that the removal efficiency is 97.23% at 50 ppm and then decreases to 92.12% at 100 ppm as shown in Fig. S12(c). In the case of MG adsorption, the removal efficiency is 79.3% at 50 ppm and then increases to 79.46% at 75 ppm and again decreases to 70.43% at 100 ppm as presented in Fig. S12(d). The influence of dye concentration on the percentage removal discloses that at less dye concentration more adsorption to adsorbent spots, thus a high percentage removal was noticed. Similarly, at higher concentrations of dyes, lower removal

efficiency was noticed because of the adsorption spots getting saturated (Bagheri et al. 2016).

**Influence of ionic strength**

The polluted groundwater and the industrial wastewater contain a large amount of salts that influence the adsorption of CV and MG. Consequently, the effect of ionic strength on the percentage removal of CV and MG onto C–Zn–Al LDH was investigated using NaCl. The salt concentration was changed from 0.2 to 0.8 mol L<sup>-1</sup>. The influence of salt ionic strength on the removal of CV and MG on to the adsorbent was given in Fig. S13. From this Figure, it can be perceived that as the salt concentration increases there was a slight variation in the dye removal efficiency of CV and MG. This can be ascribed to two main effects of sodium chloride: (i) it may confine the electrostatic interaction among the cations present in dye molecules and C–Zn–Al LDH groups increases the dye removal efficiency with increase in NaCl concentration (ii) on the other hand, it may also improve the electrostatic interaction among the cations present in dye molecules and C–Zn–Al LDH clusters through encouraging the protonation of CV and MG molecules (Wu et al. 2014; Tan et al. 2016).

**Thermodynamic studies (Van’t Hoff plot)**

The result of heat adsorption in the adsorbate on to the adsorbent particle was studied utilising the variables in thermodynamic study namely enthalpy ( $\Delta H$ ), Gibb’s energy ( $\Delta G$ ) and entropy ( $\Delta S$ ) should be considered that were calculated using Van’t Hoff equation as given below (Eqs. (7)–(8))

$$\Delta G = -RT \ln(55.5K_d) \tag{7}$$

$$\ln(55.5K_d) = \frac{\Delta S}{R} - \frac{\Delta H}{RT} \tag{8}$$

wR – universal gas constant, and K<sub>d</sub> – adsorption distribution coefficient calculated as:

$$K_d = \frac{q_e}{C_e} \tag{9}$$

where q<sub>e</sub> denotes adsorption capacity at equilibrium, C<sub>e</sub> denotes the concentration of the solution at equilibrium and 55.5 is the number of moles of water per litre of solution (Milonjić 2007; Liu 2009; Dotto et al. 2013). From Fig. S(14), the thermodynamic parameters  $\Delta S$  and  $\Delta H$  are calculated utilising the Van’t Hoff linear regression analysis with the parameters  $\ln(55.5K_d)$  vs. 1/T. The  $\Delta G$  values were negative, that denotes both CV and MG adsorption on to the C–Zn–Al LDH were spontaneous and feasible (Table 3). Positive  $\Delta H$  values (14.503 kJ/mol) were determined for MG adsorption conforming to an endothermic process, while the negative  $\Delta H$  values (–36.169 kJ/mol) were observed for CV

**Table 3** Thermodynamics parameters for the adsorption of CV and MG onto C–Zn–Al LDH

<i>T</i> (K)	$\Delta G$ (KJ mol <sup>-1</sup> )		$\Delta H$ (KJ mol <sup>-1</sup> )		$\Delta S$ (KJ mol <sup>-1</sup> K <sup>-1</sup> )	
	CV	MG	CV	MG	CV	MG
303	-16.198	-13.513	-36.169	14.503	-0.066	0.092
313	-15.054	-14.638				
323	-14.442	-15.532				
333	-14.219	-16.292				

adsorption specified an exothermic process (Rong et al. 2014; Kumari et al. 2017). The positive  $\Delta S$  values for MG adsorption revealed an enhancement in randomness at the interface of solution/solid with respect to an increase in temperature, however a reduction in randomness ensued in CV adsorption as designated by the negative  $\Delta S$  value (Mittal et al. 2010; Zhang et al. 2014a).

### Adsorption mechanism

The adsorption mechanism for CV and MG onto C–Zn–Al LDH is represented in Fig. 8a, b is explained below.

#### Electrostatic attraction

The electrostatic attraction is associated with charge nature of both adsorbent particles and contaminants. Electrostatic interaction will happen when an adsorbent particle and organic contaminants possess opposite charges; or else, electrostatic repulsion will happen if both adsorbent and organic contaminants have a similar sign of charge (Yang and Xing 2010). The maximum dye removal efficiency was obtained at pH 9 for CV and pH 6 for MG respectively. It can be inferred that C–Zn–Al LDH having negatively charged surfaces which could facilitate the electrostatic attraction of positively charged cationic dye compounds. In the adsorbent characterisation (XPS and FTIR) it was already proved that the functional group O=C–O was present in the C–Zn–Al LDH. This should be ascribed to the occurrence of electrostatic attraction between the O=C–O group present on the C–Zn–Al LDH surface and the nitrogen atom of CV and MG (Gupta and Khatri 2017; Wathukarage et al. 2017).

The surface of synthesised C–Zn–Al LDH has a point of zero charge (pHpzc) at a pH of 5.85 (Fig. S15). The surface charge of C–Zn–Al LDH displays a relationship between the pHpzc and adsorption capacity. It is significant that from the experiments, a lower pH value than the pHpzc is favourable for anion adsorption and the higher pH value than pHpzc is favourable for cation adsorption. This shows that a pH value greater than 5.85, i.e. pH > pHpzc, is influenced to have a strong electrostatic attraction between C–Zn–Al LDH and cationic dyes.

### Formation of hydrogen bond

H-bonding interaction will ensue in adsorption when carbon nanoparticles or the organic chemicals have some functional groups for example –OH, –COOH and –NH<sub>2</sub> (Yang and Xing 2010). Two categories of H-bonding interactions could happen between both dye molecule and C–Zn–Al (1) among H-donor (hydroxyl groups) on the C–Zn–Al LDH surface and H-acceptor (i.e., nitrogen) atoms in CV and MG, and (2) among aromatic rings in CV and MG and H-donor on the C–Zn–Al surface. The first Hydrogen bonding discussed is termed as dipole–dipole interaction and the second one is termed as Yoshida bonding (Tran et al. 2017a). Analysis of C–Zn–Al LDH FTIR spectra change before and after CV and MG adsorption conveys an important evidence about the adsorption mechanism. A transition to higher wavenumbers and an intensity reduction in OH peak displayed from 3294.42 to 3354.21 and 3327.21 cm<sup>-1</sup> after CV and MG adsorption; this designates the occurrence of both Yoshida and dipole-dipole H-bonding interactions and consistent with literature reports (Al-Ghouti et al. 2003; Blackburn 2004).

#### n– $\pi$ interaction

n– $\pi$  interactions were initially suggested by Mattson et al. 1969. In this interface, aromatic rings of CV and MG turn as electron acceptors whereas oxygen groups present on the C–Zn–Al surface turn as electron donors. FTIR results (Fig. 6) demonstrated a substantial reduction in the C–O peak intensity and a minor transition in the wavenumber from 1028.06 to 1083.99 and 1055.06 cm<sup>-1</sup> after CV and MG adsorption. This outcome reveals the occurrence of n– $\pi$  interactions and reliable with the previous reports (Xing et al. 1994; Nguyen et al. 2018).

#### $\pi$ – $\pi$ interaction

$\pi$ – $\pi$  interaction is applied to understand the adsorption mechanism of organic molecules with a benzene ring or a C=C bond onto the surface of carbon-coated nanoparticles since the  $\pi$ -electrons occur in the organic dye molecules act together with the  $\pi$ -electrons present in the benzene ring of carbon surface concluded the  $\pi$ – $\pi$  electron combination. Coughlin 1968 was initially suggested by this mechanism. In this study, FT-IR spectrum confirmed that peaks corresponding to C=C bonds did not show any transition in positions of wavenumber and a reduction in the intensity after adsorption of CV dye molecules. On the other hand, a significant decrease in intensity and a small shift in peak (at 1585.49 cm<sup>-1</sup>) was observed after adsorption of MG dye which ensures the  $\pi$ – $\pi$  interaction. Tran et al. 2017a concluded that peaks analogous to C=C bonds present in commercially available activated carbon,

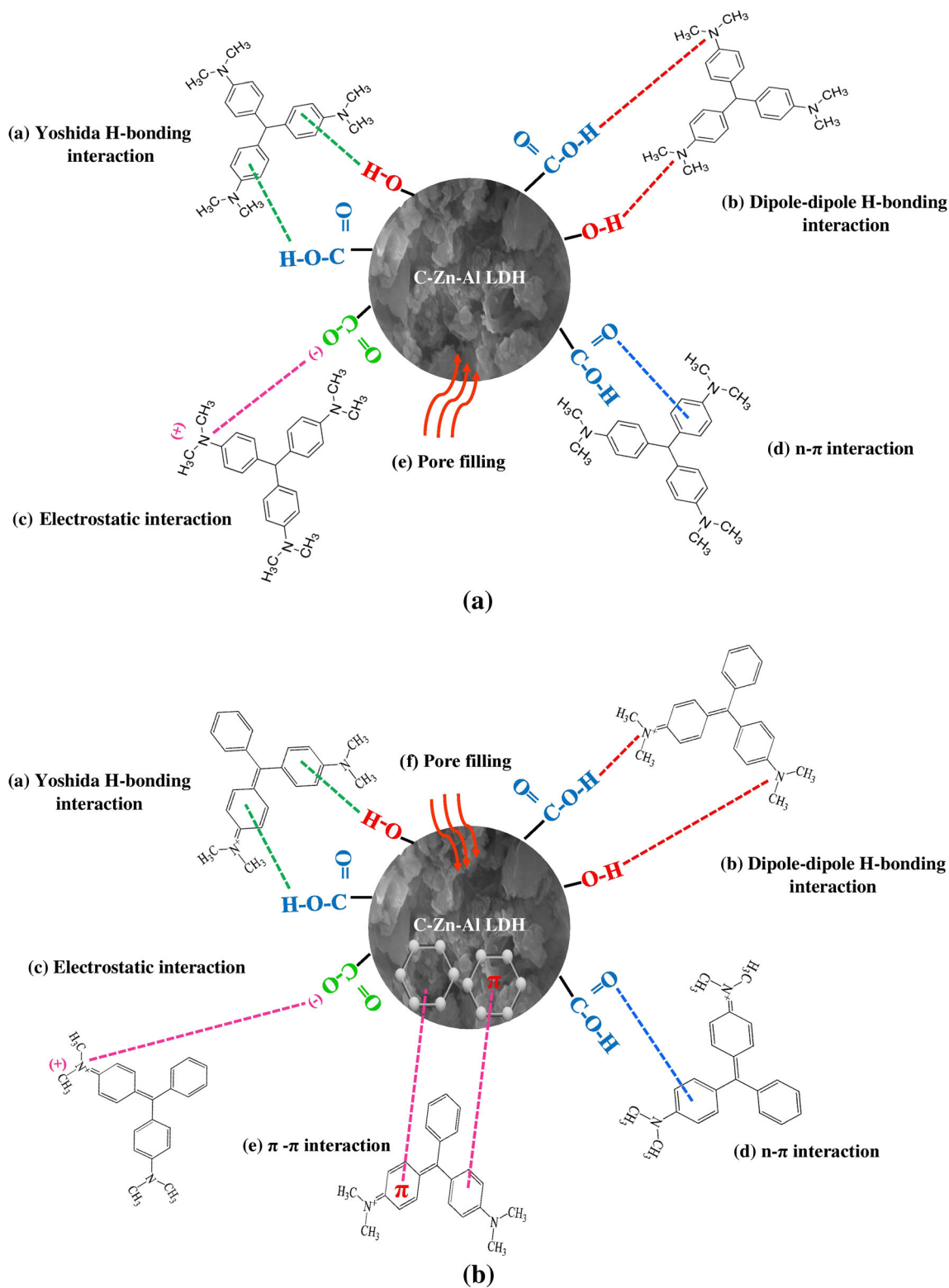


Fig. 8 Proposed adsorption mechanisms of (a) CV and (b) MG onto the C-Zn-Al LDH

the intensity is reduced and shows a shift in wavenumber after methylene green adsorption (1537 to 1561  $\text{cm}^{-1}$ ). This shift in wavenumber ensures the occurrence of  $\pi$ - $\pi$

interactions among methylene green and commercial activated carbon. Hence, the  $\pi$ - $\pi$  interactions would have not mainly influenced in the adsorption of CV whereas  $\pi$ - $\pi$

**Table 4** Comparison of the maximum adsorption capacities of various adsorbents in the removal of CV and MG dyes

Dyes	Adsorbents	$Q_m$ (mg/g)	References
Crystal violet	Activated carbon Ag nanoparticles	87.20	(AbdEl-Salam et al. 2017)
	Sodium dodecyl sulphate coated magnetic nanoparticles	166.7	(Muthukumaran et al. 2016)
	Magnetic carbon iron oxide nanocomposite	81.7	(Singh et al. 2011)
	Functionalized multi-walled carbon nanotubes	100	(Sabna et al. 2015)
	ZnO–nanorods–AC	81.6	(Dil et al. 2017)
	Chitosan–graphite oxide modified polyurethane	64.935	(Qin et al. 2015)
	<i>Terminalia arjuna</i> sawdust	45.99	(Shakoor and Nasar 2018)
	Chitin nanowhiskers	35.56	(Gopi et al. 2016)
	C–Zn–Al LDH	129.87	This work
Malachite green	Nickel hydroxide nanoplate-AC	76.92	(Agarwal et al. 2016)
	Cadmium hydroxide nanowires-AC	19	(Ghaedi and Mosallanejad 2014)
	Functionalized multi-walled carbon nanotubes	142.85	(Shirmardi et al. 2013)
	Cobalt ferrite-silica nanocomposites	75.50	(Amiri et al. 2017)
	Cr (OH) <sub>3</sub> –NPs–CNC	104	(Nekouei et al. 2017)
	Rice straw-derived char	148.74	(Hameed and El-Khaiary 2008b)
	Nitric acid treated rice husk	10.9	(Ramaraju et al. 2014)
	Defective coffee beans press cake	208.33	(Franca et al. 2010)
	C–Zn–Al LDH	126.58	This work

interactions could be one of the reasons for the removal of MG onto C–Zn–Al LDH.

### Reusability of C–Zn–Al LDH

The stability and reusability are essential for the adsorbent to be utilised as a part of practical applications. After achieving saturation adsorption of the dyes, C–Zn–Al LDH can be easily recovered by using 0.01 N NaOH solution, which has been explained in the “Experimental” section. The adsorption behaviour of C–Zn–Al LDH after repetitive use was evaluated in five consecutive CV and MG adsorption experiments. As given in Fig. S16 the dye removal efficiency decreases slightly and about 90% removal for the CV and 80% for MG was perceived after five successive cycles. The slight reduction in the removal efficiency of C–Zn–Al LDH might be ascribed to a progressive saturation of the available spots in adsorbent material. This outcome demonstrates that C–Zn–Al LDH displays a better reusability and an effective material for industrial wastewater treatment.

The comparative study between Zn–Al LDH and C–Zn–Al LDH was conducted with various dosages for the removal of CV and MG. The results of the experiments are shown in Fig. S17. It depicts that, in any given dosage, the removal efficiency of Zn–Al LDH is considerably less than that of C–Zn–Al LDH. Though various studies have proved as a promising adsorbent the H-bonding reactions among dye molecules and Zn–Al LDH played an inadequate role in dye adsorption. This is owing to the datum that only the free hydroxyl group present

in brucite sheet act as the binding spots for oxygen/nitrogen-comprising groups (Zhang et al. 2014b). Assessment of the maximum adsorption capacity of CV and MG using various adsorbents are given in Table 4. To consider the application of C–Zn–Al LDH on a large scale, the cost of this adsorbent was evaluated and represented in Table S7. It implies that the approximate cost involved in the manufacturing of C–Zn–Al LDH is economically viable for industrial applications.

### Conclusion

A new methodology for synthesising C–Zn–Al LDH via pyrolysis of glucose was demonstrated. The pyrolysis temperature (350 °C) and the mass ratio of glucose/Zn–Al LDH (0.6) were utilised for making the adsorbent material with higher adsorption capability for dye removal. The prepared Zn–Al–LDH has a hexagonal platelet structure with crystallinity, while the C–Zn–Al LDH structure was coated with carbon without diminishing the platelet shape. The maximum percentage of dye removal using C–Zn–Al LDH was observed at pH 9 & 6 for CV and MG respectively, 0.15 g/100 mL (optimum dosage) and 75 mg/L (initial dye concentration). The maximum adsorption capacity obtained from Langmuir isotherm was 129.87 mg/g for CV and 126.58 mg/g for MG. The adsorption kinetics data fits pseudo-second order kinetic models with  $R^2$  as 0.998 (CV) and 0.996 (MG) respectively. The values of  $\Delta H$  were detected to be positive (14.503 kJ/

mol) for MG adsorption conforming to an endothermic process, while in the case of CV adsorption  $\Delta H$  value was negative ( $-36.169$  kJ/mol) designated an exothermic process. The dye removal efficiencies for CV and MG were found to be 97.87 and 85.67%, signifying that C–Zn–Al LDH is an effective material for dye removal from aqueous solutions.

**Acknowledgments** The authors would like to thank Vellore Institute of Technology, Vellore Campus, for giving the necessary facilities and infrastructure to perform this work. We would also like to thank the lab staffs and technicians in fulfilling our lab needs and supplies.

## References

- Abd El-Latif MM, Ibrahim AM, El-Kady MF (2010) Adsorption equilibrium, kinetics and thermodynamics of methylene blue from aqueous solutions using biopolymer oak sawdust composite. *J Am Sci* 6: 267–283
- Abdel-Salam AH, Ewais HA, Basaleh AS (2017) Silver nanoparticles immobilised on the activated carbon as efficient adsorbent for removal of crystal violet dye from aqueous solutions. A kinetic study. *J Mol Liq* 248:833–841. <https://doi.org/10.1016/j.molliq.2017.10.109>
- Adel A, El-Zahhar NSA (2016) Removal of malachite green dye from aqueous solutions using organically modified hydroxyapatite. *J Environ Chem Eng* 4:633–638
- Agarwal S, Nekouei F, Kargarzadeh H et al (2016) Preparation of nickel hydroxide nanoplates modified activated carbon for malachite green removal from solutions: kinetic, thermodynamic, isotherm and antibacterial studies. *Process Saf Environ Prot* 102:85–97. <https://doi.org/10.1016/j.psep.2016.02.011>
- Al-Ghouti MA, Khraisheh MAM, Allen SJ, Ahmad MN (2003) The removal of dyes from textile wastewater: a study of the physical characteristics and adsorption mechanisms of diatomaceous earth. *J Environ Manag* 69:229–238. <https://doi.org/10.1016/j.jenvman.2003.09.005>
- Álvarez-Merino MA, Fontecha-Cámara MA, López-Ramón MV, Moreno-Castilla C (2008) Temperature dependence of the point of zero charge of oxidized and non-oxidized activated carbons. *Carbon* 46:778–787. <https://doi.org/10.1016/j.carbon.2008.02.002>
- Amiri M, Salavati-Niasari M, Akbari A, Gholami T (2017) Removal of malachite green (a toxic dye) from water by cobalt ferrite silica magnetic nanocomposite: herbal and green sol-gel autocombustion synthesis. *Int J Hydrog Energy* 42:24846–24860. <https://doi.org/10.1016/j.ijhydene.2017.08.077>
- Bagheri AR, Ghaedi M, Asfaram A et al (2016) Modeling and optimization of simultaneous removal of ternary dyes onto copper sulfide nanoparticles loaded on activated carbon using second-derivative spectrophotometry. *J Taiwan Inst Chem Eng* 65:212–224. <https://doi.org/10.1016/j.jtice.2016.05.004>
- Blackburn RS (2004) Natural polysaccharides and their interactions with dye molecules: application in effluent treatment. *Environ Sci Technol* 38:4905–4909. <https://doi.org/10.1021/es049972n>
- Brião GV, Jahn SL, Foletto EL, Dotto GL (2017) Adsorption of crystal violet dye onto a mesoporous ZSM-5 zeolite synthesized using chitin as template. *J Colloid Interface Sci* 508:313–322. <https://doi.org/10.1016/j.jcis.2017.08.070>
- Buvanewari N, Kannan C (2011) Plant toxic and non-toxic nature of organic dyes through adsorption mechanism on cellulose surface. *J Hazard Mater* 189:294–300. <https://doi.org/10.1016/j.jhazmat.2011.02.036>
- Chakraborty P, Nagarajan R (2015) Applied clay science Efficient adsorption of malachite green and Congo red dyes by the surfactant (DS) intercalated layered hydroxide containing Zn<sup>2+</sup>. *Appl Clay Sci* 118:308–315
- Chen H, Ai Y, Liu F et al (2016) Carbon-coated hierarchical Ni–Mn layered double hydroxide nanoarrays on Ni foam for flexible high-capacitance supercapacitors. *Electrochim Acta* 213:55–65. <https://doi.org/10.1016/j.electacta.2016.06.038>
- Cheriaa J, Khairiddine M, Rouabhia M, Bakhruf A (2012) Removal of triphenylmethane dyes by bacterial consortium. *Sci World J* 2012:1–9. <https://doi.org/10.1100/2012/512454>
- Cho S, Kim S, Oh E et al (2009) Synthesis of hierarchical hexagonal zinc oxide/zinc aluminium hydroxide heterostructures through epitaxial growth using microwave irradiation. *CrystEngComm* 11:1650. <https://doi.org/10.1039/b902130b>
- Cho D, Lee J, Sik Y et al (2016) Chemosphere fabrication of a novel magnetic carbon nanocomposite adsorbent via pyrolysis of sugar. *Chemosphere* 163:305–312. <https://doi.org/10.1016/j.chemosphere.2016.08.025>
- Coughlin RW (1968) Role of surface acidity in the adsorption of organic pollutants on the surface of carbon. *Environ Sci Technol* 2:291–297
- Crespo I, Barriga C, Rivesb V, Ulibarri MA (1997) Intercalation of iron hexacyano complexes in Zn, Al-hydrotalcite. *Solid State Ionics* 103: 729–735
- Das J, Das D, Parida KM (2006) Preparation and characterization of Mg–Al hydrotalcite-like compounds containing cerium. *J Colloid Interface Sci* 301:569–574. <https://doi.org/10.1016/j.jcis.2006.05.014>
- Del Hoyo C (2007) Layered double hydroxides and human health: an overview. *Appl Clay Sci* 36:103–121. <https://doi.org/10.1016/j.clay.2006.06.010>
- Dil EA, Ghaedi M, Asfaram A (2017) The performance of nanorods material as adsorbent for removal of azo dyes and heavy metal ions: application of ultrasound wave, optimization and modeling. *Ultrason Sonochem* 34:792–802. <https://doi.org/10.1016/j.ultrasonch.2016.07.015>
- Dos Santos VCG, De Souza JVTM, Tarley CRT et al (2011) Copper ions adsorption from aqueous medium using the biosorbent sugarcane bagasse in natura and chemically modified. *Water Air Soil Pollut* 216:351–359. <https://doi.org/10.1007/s11270-010-0537-3>
- Dotto GL, Moura JM, Cadaval TRS, Pinto LAA (2013) Application of chitosan films for the removal of food dyes from aqueous solutions by adsorption. *Chem Eng J* 214:8–16. <https://doi.org/10.1016/j.cej.2012.10.027>
- Ealias AM, Saravanakumar MP (2018) Facile synthesis and characterization of AlNs using protein rich solution extracted from sewage sludge and its application for ultrasonic assisted dye adsorption: isotherms, kinetics, mechanism and RSM design. *J Environ Manag* 206:215–227
- Ealias AM, Jose JV, Saravanakumar MP (2016) Biosynthesised magnetic iron nanoparticles for sludge dewatering via Fenton process. *Environ Sci Pollut Res* 23:21416–21430. <https://doi.org/10.1007/s11356-016-7351-4>
- El Gaini L, Lakraimi M, Sebbar E et al (2009) Removal of indigo carmine dye from water to mg–Al–CO<sub>3</sub>-calcined layered double hydroxides. *J Hazard Mater* 161:627–632. <https://doi.org/10.1016/j.jhazmat.2008.04.089>
- Elmorsi TM (2011) Equilibrium isotherms and kinetic studies of removal of methylene blue dye by adsorption onto Miswak leaves as a natural adsorbent. *J Environ Prot* 2:817–827. <https://doi.org/10.4236/jep.2011.26093>
- Evans DG, Slade CT (2006) Structural aspects of layered double hydroxides. *Struct Bond* 119:1–87. [https://doi.org/10.1007/430\\_005](https://doi.org/10.1007/430_005)
- Foo KYY, Hameed BHH (2010) Insights into the modeling of adsorption isotherm systems. *Chem Eng J* 156:2–10. <https://doi.org/10.1016/j.cej.2009.09.013>



- Franca AS, Oliveira LS, Nunes AA (2010) Malachite green adsorption by a residue-based microwave-activated adsorbent. *Clean - Soil, Air, Water* 38:843–849. <https://doi.org/10.1002/clen.201000153>
- Gaddam V, Kumar RR, Parmar M et al (2015) Morphology controlled synthesis of Al doped ZnO nanosheets on Al alloy substrate by low-temperature solution growth method. *RSC Adv* 5:13519–13524. <https://doi.org/10.1039/C4RA14049D>
- Garg VK, Gupta R, Yadav AB, Kumar R (2003) Dye removal from aqueous solution by adsorption on treated sawdust. *Bioresour Technol* 89:121–124. [https://doi.org/10.1016/S0960-8524\(03\)00058-0](https://doi.org/10.1016/S0960-8524(03)00058-0)
- Garg V, Kumar R, Gupta R (2004) Removal of malachite green dye from aqueous solution by adsorption using agro-industry waste: a case study of *Prosopis cineraria*. *Dyes Pigments* 62:1–10. [https://doi.org/10.1016/S0143-7208\(03\)00224-9](https://doi.org/10.1016/S0143-7208(03)00224-9)
- Ghaedi M, Mosallanejad N (2014) Study of competitive adsorption of malachite green and sunset yellow dyes on cadmium hydroxide nanowires loaded on activated carbon. *J Ind Eng Chem* 20:1085–1096. <https://doi.org/10.1016/j.jiec.2013.06.046>
- Ghazali A, Shirani M, Semnani A et al (2018) Optimization of crystal violet adsorption onto date palm leaves as a potent biosorbent from aqueous solutions using response surface methodology and ant colony. *J Environ Chem Eng* 6:3942–3950. <https://doi.org/10.1016/j.jece.2018.05.043>
- Gopi S, Pius A, Thomas S (2016) Enhanced adsorption of crystal violet by synthesized and characterized chitin nano whiskers from shrimp shell. *J water. Process Eng* 14:1–8. <https://doi.org/10.1016/j.jpwe.2016.07.010>
- Gupta K, Khatri OP (2017) Reduced graphene oxide as an effective adsorbent for removal of malachite green dye: plausible adsorption pathways. *J Colloid Interface Sci* 501:11–21. <https://doi.org/10.1016/j.jcis.2017.04.035>
- Hafshejania LD, Hooshmanda A, Naseria AA et al (2016) Removal of nitrate from aqueous solution by modified sugarcane bagasse biochar. *Ecol Eng* 95:101–111. <https://doi.org/10.13140/RG.2.1.4099.6243>
- Hameed BH, El-Khaiary MI (2008a) Batch removal of malachite green from aqueous solutions by adsorption on oil palm trunk fibre: equilibrium isotherms and kinetic studies. *J Hazard Mater* 154:237–244. <https://doi.org/10.1016/j.jhazmat.2007.10.017>
- Hameed BH, El-Khaiary MI (2008b) Kinetics and equilibrium studies of malachite green adsorption on rice straw-derived char. *J Hazard Mater* 153:701–708. <https://doi.org/10.1016/j.jhazmat.2007.09.019>
- Hemmati F, Norouzbeigi R, Sarbisheh F, Shayesteh H (2016) Malachite green removal using modified sphagnum peat moss as a low-cost biosorbent: kinetic, equilibrium and thermodynamic studies. *J Taiwan Inst Chem Eng* 58:482–489
- Huang J, Yang Z, Wang R et al (2015) Zn–Al layered double oxides as high-performance anode materials for zinc-based secondary battery. *J Mater Chem A* 3:7429–7436. <https://doi.org/10.1039/C5TA00279F>
- Ishikawa T, Matsumoto K, Kandori K, Nakayama T (2007) Anion-exchange and thermal change of layered zinc hydroxides formed in the presence of Al (III). *Colloids Surf A Physicochem Eng Asp* 293:135–145. <https://doi.org/10.1016/j.colsurfa.2006.07.018>
- Issa AA, Al-Degs YS, Al-Ghouti MA, Olimat AAM (2014) Studying competitive sorption behavior of methylene blue and malachite green using multivariate calibration. *Chem Eng J* 240:554–564. <https://doi.org/10.1016/j.cej.2013.10.084>
- Iwasaki M, Kita M, Ito K et al (2000) Intercalation characteristics of 1,1-diethyl-2,2-cyanine and other cationic dyes in synthetic saponite: orientation in the interlayer. *Clay Clay Miner* 48:392–399. <https://doi.org/10.1346/CCMN.2000.0480310>
- Jain S, Jayaram RV (2010) Removal of basic dyes from aqueous solution by low-cost adsorbent: wood apple shell (*Feronia acidissima*). *Desalination* 250:921–927. <https://doi.org/10.1016/j.desal.2009.04.005>
- Jenisha M, Parambadath S, Mathew A et al (2016) Highly efficient and selective adsorption of in 3+ on pristine Zn / Al layered double hydroxide (Zn/Al-LDH) from aqueous solutions. *J Solid State Chem* 233:133–142
- Jha SK, Yoon TH, Pan Z (2018) Multivariate statistical analysis for selecting optimal descriptors in the toxicity modeling of nanomaterials. *Comput Biol Med* 99:161–172. <https://doi.org/10.1016/j.compbiomed.2018.06.012>
- Kim Y, Yang W, Liu PKT et al (2004) Thermal evolution of the structure of a mg - Al - CO 3 layered double hydroxide: sorption reversibility aspects. *Ind Eng Chem Res* 43:4559–4570
- Kim H, Kang S, Park S, Seok H (2015) Journal of industrial and engineering chemistry adsorption isotherms and kinetics of cationic and anionic dyes on three-dimensional reduced graphene oxide macrostructure. *J Ind Eng Chem* 21:1191–1196. <https://doi.org/10.1016/j.jiec.2014.05.033>
- Konicki W, Aleksandrak M, Moszyński D, Mijowska E (2017) Adsorption of anionic azo-dyes from aqueous solutions onto graphene oxide: equilibrium, kinetic and thermodynamic studies. *J Colloid Interface Sci* 496:188–200. <https://doi.org/10.1016/j.jcis.2017.02.031>
- Kumari HJ, Krishnamoorthy P, Arumugam TK et al (2017) International journal of biological macromolecules an efficient removal of crystal violet dye from waste water by adsorption onto TLAC/chitosan composite: a novel low cost adsorbent. *Int J Biol Macromol* 96:324–333. <https://doi.org/10.1016/j.ijbiomac.2016.11.077>
- Laskar N, Kumar U (2018) Adsorption of crystal violet from wastewater by modified Bambusa Tulda. *KSCE J Civ Eng* 22:2755–2763. <https://doi.org/10.1007/s12205-017-0473-5>
- Lee S, Zhang Z, Wang X et al (2011) Characterization of multi-walled carbon nanotubes catalyst supports by zero charge. *Catal Today* 164:68–73. <https://doi.org/10.1016/j.cattod.2010.10.031>
- Liu Y (2009) Is the free energy change of adsorption correctly calculated? *J Chem Eng Data* 54:1981–1985. <https://doi.org/10.1021/je800661q>
- Liu Z, Ma R, Osada M, Iyi N, Ebina Y, Takada K, Sasaki T (2006) Synthesis, anion exchange, and delamination of co - Al layered double hydroxide: assembly of the exfoliated nanosheet/polyanion composite films and magneto-optical studies. *JACS Artic* 128:4872–4880
- Lu D, Gao Q, Wu X, Fan Y (2017) ZnO nanostructures decorated hollow glass microspheres as near infrared reflective pigment. *Ceram Int* 43:0–1. <https://doi.org/10.1016/j.ceramint.2017.04.067>
- Marangoni R, Ramos LP, Wypych F (2000) Covalent grafting of ethylene glycol into the Zn - Al - CO 3 layered double hydroxide. *J Colloid Interface Sci* 227:445–451. <https://doi.org/10.1006/jcis.2000.6873>
- Mashkour F, Nasar A, Inamuddin AAM (2018) Exploring the reusability of synthetically contaminated wastewater containing crystal violet dye using tectona grandis sawdust as a very low-cost adsorbent. *Sci Rep* 8:1–16. <https://doi.org/10.1038/s41598-018-26655-3>
- Mattson JA, Mark HB, Malbin MD et al (1969) Surface chemistry of active carbon: specific adsorption of phenols. *J Colloid Interface Sci* 31:116–130. [https://doi.org/10.1016/0021-9797\(69\)90089-7](https://doi.org/10.1016/0021-9797(69)90089-7)
- Menendez JA, Gomez I, Leon L, Radovic LR (1995) On the difference between the isoelectric point and the point of zero charge of carbons. *Carbon* 33:1655–1659
- Milonjić SK (2007) A consideration of the correct calculation of thermodynamic parameters of adsorption. *J Serbian Chem Soc* 72:1363–1367. <https://doi.org/10.2298/JSC0712363M>
- Mittal A, Mittal J, Malviya A et al (2010) Adsorption of hazardous dye crystal violet from wastewater by waste materials. *J Colloid Interface Sci* 343:463–473. <https://doi.org/10.1016/j.jcis.2009.11.060>
- Mustapha M, Derriche Z, Denoyel R et al (2011) Thermodynamical and structural insights of orange II adsorption by Mg R AINO 3 layered

- double hydroxides. *J Solid State Chem* 184:1016–1024. <https://doi.org/10.1016/j.jssc.2011.03.018>
- Muthukumar C, Sivakumar VM, Thirumarimurugan M (2016) Adsorption isotherms and kinetic studies of crystal violet dye removal from aqueous solution using surfactant modified magnetic nano-adsorbent. *J Taiwan Inst Chem Eng* 63:354–362. <https://doi.org/10.1016/j.jtice.2016.03.034>
- Nekouei F, Nekouei S, Keshtpour F et al (2017) Cr (OH)<sub>3</sub>-NPs-CNC hybrid nanocomposite: a sorbent for adsorptive removal of methylene blue and malachite green from solutions. *Environ Sci Pollut Res* 24. <https://doi.org/10.1007/s11356-017-0111-2>
- Nguyen H, You S, Chao H (2018) Fast and efficient adsorption of methylene green 5 on activated carbon prepared from new chemical activation method. *J Environ Manag* 188:322–336. <https://doi.org/10.1016/j.jenvman.2016.12.003>
- Prasanna SV, Kamath PV (2008) Chromate uptake characteristics of the pristine layered double hydroxides of Mg with Al. *Solid State Sci* 10: 260–266. <https://doi.org/10.1016/j.solidstatesciences.2007.09.023>
- Qin J, Qiu F, Rong X et al (2015) Adsorption behavior of crystal violet from aqueous solutions with chitosan-graphite oxide modified polyurethane as an adsorbent. *J Appl Polym Sci* 132:1–10. <https://doi.org/10.1002/app.41828>
- Ramaraju B, Reddy PMK, Subrahmanyam C (2014) Low cost adsorbents from agricultural waste for removal of dyes. *Environ Prog Sustain Energy* 33:38–46. <https://doi.org/10.1002/ep.11742>
- Rong X, Qiu F, Qin J et al (2014) Journal of industrial and engineering chemistry removal of malachite green from the contaminated water using a water-soluble melamine/maleic anhydride sorbent. *J Ind Eng Chem* 20:3808–3814. <https://doi.org/10.1016/j.jiec.2013.12.083>
- Ryu S, Jung H, Oh J et al (2010) Journal of physics and chemistry of solids layered double hydroxide as novel antibacterial drug delivery system. *J Phys Chem Solids* 71:685–688. <https://doi.org/10.1016/j.jpcs.2009.12.066>
- Sabna V, Thampi SG, Chandrakaran S (2015) Ecotoxicology and environmental safety adsorption of crystal violet onto functionalised multi-walled carbon nanotubes: equilibrium and kinetic studies. *Ecotoxicol Environ Saf* 1–8. <https://doi.org/10.1016/j.ecoenv.2015.09.018>
- Sartape AS, Mandhare AM, Jadhav VV et al (2017) Removal of malachite green dye from aqueous solution with adsorption technique using *Limonia acidissima* (wood apple) shell as low cost adsorbent. *Arab J Chem* 10:3229–3238
- Schwantes D, Gonçalves AC, Coelho GF et al (2016) Chemical modifications of cassava peel as adsorbent material for metals ions from wastewater. *J Chem* 2016. <https://doi.org/10.1155/2016/3694174>
- Shakoor S, Nasar A (2018) Adsorptive decontamination of synthetic wastewater containing crystal violet dye by employing *Terminalia arjuna* sawdust waste. *Groundw Sustain Dev*. <https://doi.org/10.1016/j.memsci.2015.12.065>
- Shan R, Yan L, Yang Y et al (2015) Highly efficient removal of three red dyes by adsorption onto Mg – Al-layered double hydroxide. *J Ind Eng Chem* 21:561–568
- Sharifpour E, Haddadi H, Ghaedi M (2017) Optimization of simultaneous ultrasound assisted toxic dyes adsorption conditions from single and multi-components using central composite design: application of derivative spectrophotometry and evaluation of the kinetics and is. *Ultrason Sonochem* 36:236–245
- Shirmardi M, Mahvi AH, Hashemzadeh B et al (2013) The adsorption of malachite green (MG) as a cationic dye onto functionalized multi walled carbon nanotubes. *Korean J Chem Eng* 30:1603–1608. <https://doi.org/10.1007/s11814-013-0080-1>
- Singh KP, Gupta S, Singh AK, Sinha S (2011) Optimizing adsorption of crystal violet dye from water by magnetic nanocomposite using response surface modeling approach. *J Hazard Mater* 186:1462–1473. <https://doi.org/10.1016/j.jhazmat.2010.12.032>
- Tan X, Liu Y, Gu Y et al (2016) Biochar pyrolyzed from MgAl-layered double hydroxides pre-coated ramie biomass (*Boehmeria nivea* (L.) Gaud.): characterization and application for crystal violet removal. *J Environ Manag* 184:85–93
- Tran HN, Wang Y-F, You S-J, Chao H-P (2017a) Insights into the mechanism of cationic dye adsorption on activated charcoal: the importance of  $\pi$ - $\pi$  interactions. *Process Saf Environ Prot* 107:168–180. <https://doi.org/10.1016/j.psep.2017.02.010>
- Tran HN, You SJ, Chao HP (2017b) Insight into adsorption mechanism of cationic dye onto agricultural residues-derived hydrochars: negligible role of  $\pi$ - $\pi$  interaction. *Korean J Chem Eng* 34:1708–1720. <https://doi.org/10.1007/s11814-017-0056-7>
- Vial S, Prevot V, Leroux F, Forano C (2008) Immobilization of urease in ZnAl layered double hydroxides by soft chemistry routes. *Microporous Mesoporous Mater* 107:190–201. <https://doi.org/10.1016/j.micromeso.2007.02.033>
- Wang SL, Hseu RJ, Chang RR et al (2006) Adsorption and thermal desorption of Cr (VI) on Li/Al layered double hydroxide. *Colloids Surf A Physicochem Eng Asp* 277:8–14. <https://doi.org/10.1016/j.colsurfa.2005.10.073>
- Wang Y, Zhang F, Xu S et al (2008) Preparation of layered double hydroxide microspheres by spray drying. *Ind Eng Chem Res* 47:5746–5750
- Wathukarage A, Herath I, Iqbal MCM, Vithanage M (2017) Mechanistic understanding of crystal violet dye sorption by woody biochar: implications for wastewater treatment. *Environ Geochem Health* 1–15. <https://doi.org/10.1007/s10653-017-0013-8>
- Wu P, Wu T, He W et al (2013) Adsorption properties of dodecylsulfate-intercalated layered double hydroxide for various dyes in water. *Colloids Surf A Physicochem Eng Asp* 436:726–731. <https://doi.org/10.1016/j.colsurfa.2013.08.015>
- Wu Z, Zhong H, Yuan X, Wang H (2014) Adsorptive removal of methylene blue by rhamnolipid-functionalized graphene oxide from wastewater. *Water Res* 67:330–344
- Xiangliang Pan DZ (2009) Removal of malachite green from water by *Firmiana simplex* wood fiber. *Electron J Biotechnol* 12:1–10. <https://doi.org/10.2225/vol12-issue4-fulltext-4>
- Xing B, McGill WB, Dudas MJ et al (1994) Sorption of phenol by selected biopolymers: isotherms, energetics, and polarity. *Environ Sci Technol* 28:466–473. <https://doi.org/10.1021/es00052a019>
- Yan L-G, Yang K, Shan R-R et al (2015) Calcined ZnAl- and Fe<sub>3</sub>O<sub>4</sub>/ZnAl-layered double hydroxides for efficient removal of Cr (vi) from aqueous solution. *RSC Adv* 5:96495–96503. <https://doi.org/10.1039/c5ra17058c>
- Yang K, Xing B (2010) Adsorption of organic compounds by carbon nanomaterials in aqueous phase: polanyi theory and its application. *Chem Rev* 110:5989–6008. <https://doi.org/10.1021/cr100059s>
- Yang K, Yan L, Yang Y et al (2014) Adsorptive removal of phosphate by Mg – Al and Zn – Al layered double hydroxides: kinetics, isotherms and mechanisms. *Sep Purif Technol* 124:36–42. <https://doi.org/10.1016/j.seppur.2013.12.042>
- Yang S, Wang L, Zhang X et al (2015) Enhanced adsorption of Congo red dye by functionalized carbon nanotube/mixed metal oxides nanocomposites derived from layered double hydroxide precursor. *Chem Eng J* 275:315–321
- Zahra F, Khalidi A, Abdennouri M et al (2017) Zn–Al layered double hydroxides intercalated with carbonate, nitrate, chloride and sulphate ions: synthesis, characterisation and dye removal properties. *J Taibah Univ Sci* 11:90–100. <https://doi.org/10.1016/j.jtusc.2015.10.007>
- Zhang Y, Pan Q, Chai G et al (2013) Synthesis and luminescence mechanism of multicolor-emitting g-C<sub>3</sub>N<sub>4</sub> nanopowders by low temperature thermal condensation of melamine. *Sci Rep* 3:1–8. <https://doi.org/10.1038/srep01943>
- Zhang L, Zhang H, Guo W, Tian Y (2014a) Removal of malachite green and crystal violet cationic dyes from aqueous solution using activated sintering process red mud. *Appl Clay Sci* 94:85–93

- Zhang M, Yao Q, Lu C et al (2014b) Layered double hydroxide – carbon dot composite: high- performance adsorbent for removal of anionic organic dye. *ACS Appl Mater Interfaces* 6:20225–20233. <https://doi.org/10.1021/am505765e>
- Zhang F, Wei Z, Zhang W, Cui H (2017) Effective adsorption of malachite green using magnetic barium phosphate composite from aqueous solution. *Spectrochim Acta A Mol Biomol Spectrosc* 182:116–122. <https://doi.org/10.1016/j.saa.2017.03.066>
- Zhao H, Lang Y (2018) Adsorption behaviors and mechanisms of florfenicol by magnetic functionalized biochar and reed biochar. *J Taiwan Inst Chem Eng* 88:152–160. <https://doi.org/10.1016/j.jtice.2018.03.049>
- Zhao Y, Li N, Xu B et al (2016) Preparation and characterization of a novel hydrophilic poly (vinylidene fluoride) filtration membrane incorporated with Zn–Al layered double hydroxides. *J Ind Eng Chem* 39:37–47. <https://doi.org/10.1016/j.jiec.2016.05.006>
- Zheng Y, Li N, Zhang W (2012) Preparation of nanostructured microspheres of Zn – Mg – Al layered double hydroxides with high adsorption property. *Colloids Surf A Physicochem Eng Asp* 415: 195–201. <https://doi.org/10.1016/j.colsurfa.2012.10.014>